SANDIA REPORT

SAND2011-3779
Unlimited Release
Printed June 2011

The Sandia 100-meter All-glass Baseline Wind Turbine Blade: SNL100-00

D. Todd Griffith and Thomas D. Ashwill

Prepared by
Sandia National Laboratories
Albuquerque, New Mexico 87185 and Livermore, California 94550

Sandia National Laboratories is a multi-program laboratory managed and operated by Sandia Corporation, a wholly owned subsidiary of Lockheed Martin Company, for the U.S. Department of Energy's National Nuclear Security Administration under Contract DE-AC04-94AL85000.

Issued by Sandia National Laboratories, operated for the United States Department of Energy by Sandia Corporation.

Available to DOE and DOE contractors from
U.S. Department of Energy
Office of Scientific and Technical Information
P.O. Box 62
Oak Ridge, TN 37831

Telephone: (865) 576-8401
Facsimile: (865) 576-5728
E-Mail: reports@adonis.osti.gov
Online ordering: http://www.osti.gov/bridge

Available to the public from
U.S. Department of Commerce
National Technical Information Service
5285 Port Royal Rd.
Springfield, VA 22161

Telephone: (800) 553-6847
Facsimile: (703) 605-6900
E-Mail: orders@ntis.fedworld.gov
Online order: http://www.ntis.gov/help/ordermethods.asp?loc=7-4-0#online

SAND2011-3779
Unlimited Release
Printed June 2011

THE SANDIA 100-METER ALL-GLASS BASELINE WIND TURBINE BLADE: SNL100-00

D. Todd Griffith
Analytical Structural Dynamics Department

Thomas D. Ashwill
Wind Energy Technologies Department

Sandia National Laboratories
P.O. Box 5800
Albuquerque, New Mexico 87185-0557

Abstract

Sandia National Laboratories (SNL) Wind Energy Technologies Department, as part of its ongoing R&D efforts, creates and evaluates innovative large blade concepts for horizontal axis wind turbines to promote designs that are more efficient aerodynamically, structurally, and economically. Recent work has focused on the development of a 100-meter blade for a 13.2 MW horizontal axis wind turbine, a blade which is significantly longer than the largest commercial blades of today (approximately 60 meters long). This report documents the development of the Sandia 100-m All-glass Baseline Wind Turbine Blade, which employs conventional architecture and fiberglass-only composite material reinforcement. Follow-on studies for this baseline will include a variety of innovations targeting reductions in weight and improvements in structural and aerodynamic performance.

The report begins with a review of several large utility-grade machines (3-6 MW). Available 5 MW turbine models (with 61.5 meter blades) are identified and described. Geometric scaling of these models is performed to produce aeroelastic turbine models with 100-meter blades, which are analyzed to demonstrate the important effects of scale for large blades. Based on these preliminary analyses, we proceed to develop the Sandia 100-m all-glass baseline blade model. A detailed composite layup and geometry are provided. Analyses of the baseline model for design loads from international standards are presented to demonstrate acceptance of the design with respect to strength, fatigue, deflection, and buckling. In future work, it is envisioned that this model will provide a starting point for consideration of blade innovations with potential performance and cost improvements and will be targeted toward the offshore environment.

Acknowledgments

The authors would like to acknowledge Brian Resor, Sandia Labs, who provided significant contributions in performing the calculations to determine the blade fatigue life and in compiling a new controller for the 13.2 MW FAST turbine model. We're grateful to Jonathan Berg, Sandia Labs, for providing an updated version of the PreComp code, which was used to perform the cross section analyses performed throughout this report. The authors would like to acknowledge helpful discussions with Kevin Jackson, Dynamic Design, regarding international design standards, and Mike Zuteck, MDZ Engineering, regarding blade manufacturing considerations.

Contents

Figures

Tables

1.0 Overview of Large Blade Development Project

A dominant and consistent trend in commercial utility-grade wind turbine production throughout the years has been growth in the size of the rotor and lowered cost-of-energy. Advancements in blade design technology have been achieved through more efficient structural and aerodynamic designs and optimal material usage. Earlier WindPACT studies investigated and evaluated design, materials and manufacturing issues for large wind turbine blades and rotors that resulted in design specifications and preliminary designs for candidate blades in the range of 30 to 70 meters in length [1,2] and rotors in the range of 80 to 120 meters in diameter [2,3]. Future designs for even larger machines will continue to push the extremes of the design envelope, which is primarily limited by the penalty of weight growth.

The focus of the work reported here is the development of a very large (100-m) glass baseline blade that will serve as a platform for understanding a variety of modern innovations with the potential to enable cost-effective, large turbine designs of 13.2 MW and beyond. A number of innovations already identified include the effect of new and improved materials, blade architecture, and manufacturing approaches.

The report begins with a review of state-of-the-art large utility-grade machines. Descriptions of existing, available 5 MW turbine models (with 61.5 meter blades) are discussed. Geometric scaling of these available models was performed to produce aeroelastic turbine models with 100-meter blades, which were analyzed to demonstrate the important effects of scale for large blades. Based on these preliminary analyses, we proceeded to develop a large blade baseline model which is designated as the "Sandia 100-m All-glass Baseline Blade: SNL100-00". A detailed composite layup and geometry are determined. Analyses of the baseline model for design loads from international standards are presented to demonstrate acceptance of the design with respect to strength, fatigue, deflection, and buckling considerations. In future work, it is envisioned that this model will provide a starting point for consideration of blade innovations to evaluate potential performance and cost improvements and will be targeted to the offshore environment.

1.1 State of the Art of Large Turbines

At the onset of this research, blades on the largest installed machines in the world had a length of 61.5 meters. Table 1 lists the largest prototypes or available machines from several turbine manufacturers (web survey conducted on January 25, 2011). These machines have ratings of 2.5 to 6.15 MW with rotor diameters up to 128 meters. The survey is not intended to be exhaustive by any means, but lists information readily available to the public.

Manufacturers are making plans for the development of even larger machines. For example, the publicly announced Clipper Britannia Project is planning for the design of a machine rated at 10 MW. Other large blade studies include the work of Hillmer in 2007 [4], where the authors explore the effect of scale in blade design for blades up to 82 meters in length.

Table 1. Current Status of Large Turbines

Manufacturer	Machine Rating	Siting	Rotor Diameter	Comments
Acciona	3.0 MW	Onshore/Offshore	116 m	
Clipper	2.5 MW	Onshore	99 m	
Enercon	6.0 MW	Onshore	126 m	Direct Drive
Gamesa	4.5 MW	Onshore	128 m	
GE	4.0 MW	Offshore	110 m	Direct Drive
Multibrid	5.0 MW	Offshore	116 m	
RePower	6.15 MW	Onshore/Offshore	126 m	
Siemens	3.6 MW	Onshore/Offshore	107 m	
Vestas	3.0 MW	Onshore/Offshore	112 m	

1.2 Existing/Available Models

In order to perform structural analysis for evaluating design trade-offs, realistic structural models are needed. Technical data from manufacturers is, of course, very limited. Distributed structural model properties from studies of large turbines and blades are only available from previous independent, "public" studies, e.g. the DOWEC (Dutch Offshore Wind Energy Converter) study [5, 6], the UpWind Project [7], and DOE/NREL work [8]. These studies focused on turbines with ratings of 5-6 MW and blade lengths in the range of 61.5 to 64.5 meters.

1.2.1 DOWEC Blade Study

The DOWEC study [5,6] was conducted from 1997-2003 and included the development of a 64.5 meter blade. Among other results, this blade research study reported distributed blade mass and stiffness properties as well as distributed geometric properties (i.e. chord and airfoil schedules). Both the DOE/NREL 5 MW model [8] and the UpWind project [7] utilized data from the 64.5 meter blade development study of the DOWEC consortium [5, 6].

1.2.2 NREL 5 MW FAST Aeroelastic Model

An aeroelastic model of a 5 MW turbine was developed at NREL (February 2009) by surveying the available conceptual designs and existing designs of similar size [8]. The NREL 5 MW model was analyzed using the FAST aeroelastic code [9]. This 5 MW turbine model has been made widely available to wind energy researchers for research studies. The turbine model contains distributed properties for the tower and blades and includes models for the nacelle and drive train dynamics. Also, controllers were developed for the NREL 5 MW turbine, which include yaw, variable speed, and collective pitch control characteristics (in addition to standard controllers already available in the FAST code). The NREL 5 MW turbine model used the DOWEC structural and aerodynamic properties for its blades, although the blade was truncated to 61.5 meters from the original 64.5 meters.

1.2.3 UpWind 5 MW Composite Layup

The UpWind Project is a comprehensive research program with a primary focus on large blades. As part of the study, UpWind researchers created an all-glass 61.5 meter blade design with the same external geometry (airfoil and chord schedules) as the DOWEC 64.5 meter blade. Due to the proprietary

nature of the DOWEC study, its layup data was not made publicly available. Therefore, UpWind researchers developed a material layup independently [10].

1.3 Objectives of Research

The objectives of this research are to investigate the opportunities and limitations for very large blade technology. Our approach is to use structural analysis to evaluate conventional and new design concepts. We start this process by examining existing models which best represent state-of-art of large machines. These models are used as baselines for scaling to larger machines followed by the development and documentation of a composite layup for a 100-m blade. This work will add new information to the public knowledge base regarding the design approach and trends for large blade technology.

The major sections of the report are as follows. In Section 2.0, equations for blade and turbine property scaling and trends in design drivers are presented. Included is summary data for existing state-of-the-art large turbines and results of scaling existing 5 MW models to turbines as large as 15 MW. In Section 3.0, up-scaled 13.2 MW turbine models with 100-m blades are analyzed. These preliminary results guide the detailed design for the Sandia 100-m All-glass Baseline Blade, which is presented in Section 4.0. Section 4.0 also includes a detailed composite layup definition with blade geometry. Analyses based on international design standards are reported to demonstrate the structural performance of the design.

2.0 Scaling Laws for Blade Structural Properties and Design Trends

Scaling laws can be used to extrapolate existing model properties to larger turbine sizes and predict the effect of blade length on design trends such as root bending moments and natural frequencies. In this section we consider general scaling trends. Later in this report, we apply these laws to scale a 5 MW turbine with a 61.5 meter blade to larger turbine and blade sizes.

2.1 Scaling Laws

Conventional scaling of turbine and blade properties is accomplished by a dimensional analysis, whereby all length dependent variables are scaled according to a scale factor. Scaling laws, based on this dimensional analysis, can be developed for turbine power, blade mass and stiffness properties, root bending moments and other turbine mass properties. In addition to geometric similarity, material similarity and constant tip speed ratio are assumed for this conventional up-scaling.

First, we define a scale factor, α, as the ratio of the scaled blade length (L_U) to the nominal blade length (L_B):

$$\alpha = \frac{Scaled\ Length}{Nominal\ Length} = \frac{L_U}{L_B} \tag{1}$$

where "U" refers to the up-scaled blade and "B" refers the nominal blade. Alternatively, the scale factor can be defined as the ratio of the scaled rotor radius to the nominal rotor radius.

The total blade mass follows this relationship:

$$m_U = \alpha^3 m_B \tag{2}$$

and the rotor power:

$$P_U = \alpha^2 P_B \tag{3}$$

We immediately observe the well-known fact that as blade length increases blade mass grows at a faster rate (α^3) than rotor power (α^2). Innovations can be utilized to reduce the rate of mass growth. Equation (2) is the result of volume scaling because the material density is held constant due to assumed material similarity. Rotor power depends on the swept area of the rotor, thus the squared relationship in Equation (3).

Further, the CG location, z, of the blade (or any span-wise location on the blade for that matter) follows the following scaling law:

$$z_U = \alpha^1 z_B \tag{4}$$

Scaling laws can also be developed for the blade response to loads. For example, root bending moments, which are important design drivers, can be written with scaling laws. Expressions for the root

bending moments that result from aerodynamic forces or gravitational loads are given below (Eqs. 7,8). The aerodynamic lift and drag forces can be written as [11]:

$$F_L = \tfrac{1}{2}\rho A C_L V^2 \tag{5}$$

$$F_D = \tfrac{1}{2}\rho A C_D V^2 \tag{6}$$

where ρ is air density, A is area, C_L and C_D are aerodynamic coefficients, and V is velocity. Both expressions for the aerodynamic force have the same mathematical form. The velocity depends on the inflow wind speed as well as the rotational rate. When assuming constant tip speed ratio for up-scaling, the velocity field along the blade is a constant. In order to maintain constant tip speed for longer blades, the turbine operating speed is reduced linearly. Area, then, is the only variable dependent on scale in these equations, thus aerodynamic forces, both lift and drag, scale with the square of the scale factor.

We now consider bending moments due to aerodynamic loads. The bending moments arise from the product of force on the blade elements (an α^2 dependence) and the span-wise location of the applied load (an α^1 dependence). Thus, moments due to aerodynamic loads are scaled by the following cubic relation:

$$M_U^{Aero} = \alpha^3 M_B^{Aero} \tag{7}$$

We now consider root bending moments due to gravitational loads. These moments arise from the product of blade weight and its span-wise location. For conventional up-scaling, blade mass grows as the cube of the scale factor (See Equation 2) while location scales linearly. Therefore, moments due to gravitational loads grow with the fourth power of the scale factor:

$$M_U^{Gravity} = \alpha^4 M_B^{Gravity} \tag{8}$$

Thus, we can see from Equations 7 and 8 that moments due to gravitational loads scale at a faster rate than aerodynamic loads. For blades on today's machines, aerodynamic loads are typically larger than gravitational loads. Thus, root bending moments due to aerodynamic loads have been a principal design driver especially in the flap-wise direction. However, it is clear that as blade length increases, root bending moments due to gravitational loads will grow to exceed moments due to aerodynamic loads. Gravity loads are primarily resisted in the lead-lag direction. Much larger gravity loading will require additional reinforcement and design adjustments in the lead-lag direction and beefed up components all the way through the turbine system itself.

The root bending moment relations can be re-written in terms of stress or strain. One finds that stress (and strain) due to aerodynamic loads is independent of scale (α^0). On the other hand, stress (and strain) due to gravitational loads grow linearly (α^1) with scale. Observing these trends is important for strength and fatigue calculations, and demonstrates important design considerations for edge-wise strains.

The natural frequencies of blade bending modes drop linearly with the scale factor (an α^{-1} dependence). This trend can be observed by considering an analytical formula for the natural frequency of a beam with uniform cross-section:

$$f_i = \frac{\lambda_i^2}{2\pi L^2}\sqrt{\frac{EI}{\rho A}} \tag{9}$$

where λ_i is a constant associated with the ith mode, L is the beam length, E is Young's Modulus, I is the area moment of inertia, ρ is density, and A is cross-sectional area.

With material similarity, E and ρ, are held constant while only the geometric variables are scaled. The result is

$$\begin{aligned} f_i^U &= \frac{1}{\alpha}\frac{\lambda_i^2}{2\pi L^2}\sqrt{\frac{EI}{\rho A}} \\ &= \frac{1}{\alpha} f_i^B \end{aligned} \tag{10}$$

However, on a per rev basis natural frequencies (natural frequency divided by the operating speed) are independent of scale because the operating speed also scales as α^{-1} .

2.2 Results of Blade and Turbine Scaling for Existing Model Data

To analyze operating cases for a 100-m blade model, it is necessary to also develop the underlying turbine model, which is 13.2 MW in size. The turbine model and initial 100-m blade model are created by scaling up existing 5 MW blade and turbine models. In this section, existing 5 MW blade and turbine models are reviewed. First, published data for blade geometry from the DOWEC study is listed. Then, structural model details for the NREL 5 MW turbine model and the UpWind 5 MW composite layup are presented. The approach uses existing blade geometry data from the DOWEC study and composite layup data from the UpWind program in our preliminary 5 MW baseline blade model developments. The NREL 5 MW turbine model properties are scaled to provide a 13.2 MW turbine model which serves as a means to evaluate different blade models, including upscaled versions of DOWEC and UpWind blades, for a variety of IEC load cases.

2.2.1 DOWEC Study Airfoils and Chord Schedule

The airfoils and chord schedule used in the development of 61.5 meter models in the NREL study and apparently also the UpWind study [10] were adopted from the DOWEC study [5,6]. The development of the Sandia 100-meter All-glass Baseline Blade adopts the same DOWEC airfoil and chord schedules to define blade external geometry as aerodynamic performance was not part of this design study. The chord schedule reported by DOWEC is plotted in Figure 1. The maximum chord location is approximately at 20% of the blade span.

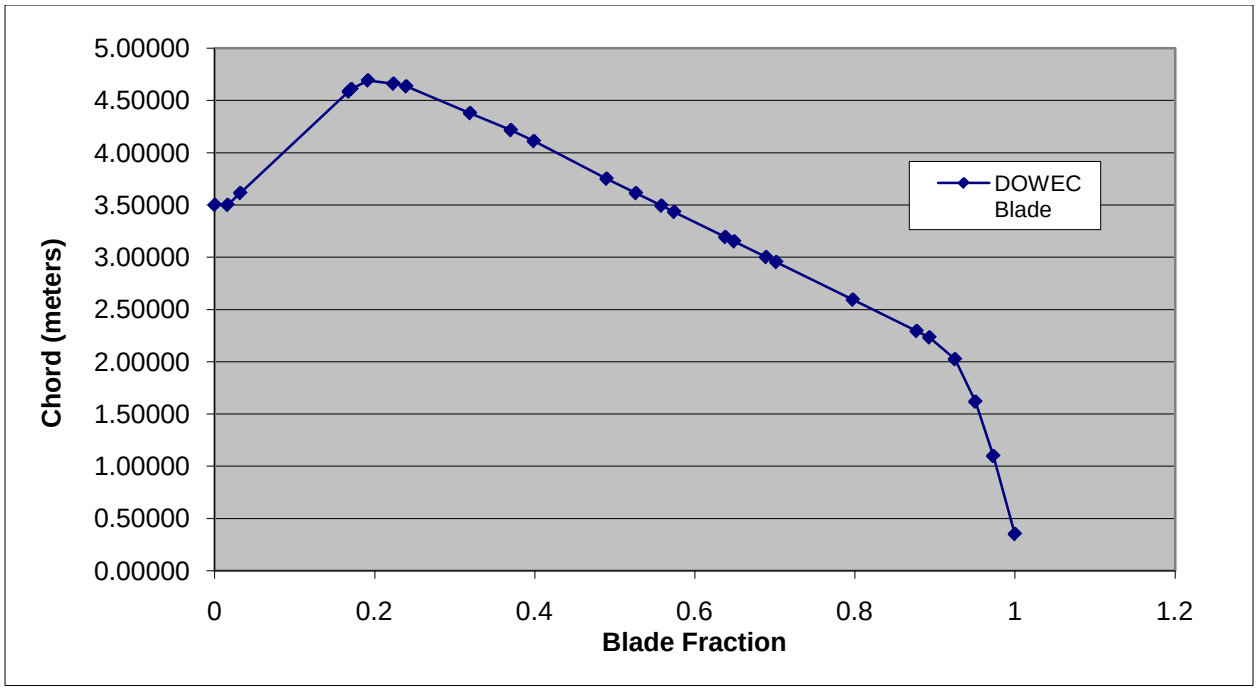

Figure 1. Chord Schedule for DOWEC 64.5 Meter Blade

The reported DOWEC airfoil schedule is listed in Table 2. The TU-Delft family of airfoils was used with thickness to chord (t/c) ratios of 40.5% at maximum chord down to 21% at approximately 2/3 span. NACA 64-series airfoils were used in the final one-third blade span. No transition airfoils were reported between the root circle and airfoil at maximum chord and had to be developed for the 100-m baseline geometry.

Table 2. Airfoil Schedule for DOWEC 64.5 Meter Blade

Airfoil Designation	Thickness (t/c)	Begin Radius (m)	End Radius (m)
Cylinder1	100%	1.8	5.98
Cylinder2	100%	5.98	10.15
DU40_A17	40.5%	10.15	15.00
DU35_A17	35.09%	15.00	20.49
DU30_A17	30%	20.49	26.79
DU25_A17	25%	26.79	34.22
DU21_A17	21%	34.22	42.47
NA64_A17	18%	42.47	64.50

2.2.2 NREL 5 MW Aeroelastic Turbine Model

The NREL 5MW model (61.5 meter blade) is a complete turbine model, and therefore, each turbine component can be used in these scaling studies. The blade data, adopted from the DOWEC report [6] includes detailed distributed span-wise properties: structural twist, mass per unit length, flap-wise and edge-wise bending stiffness, and axial and torsional stiffness. No actual laminate schedule or lay-up details are provided. The distributed span-wise properties are defined at approximately 0.5 to 1 meter intervals within the model for the 61.5 meter blade. Conventional scaling assumes material similarity; therefore, Young's Modulus and density are constants. Thus, scaling of cross-sectional stiffness properties depends completely on geometry. Bending and torsional stiffness values scale with the fourth power of the scale factor, while axial stiffness values scale with the second power of the scale factor.

The mass and stiffness distributions for the 5 MW model and up-scaled models to ratings of 10, 13.2 and 15 MW are given in Figures 2 through 4. The structural twist was not changed in the scale up because it does not depend on length variables. Blade mass per unit length was scaled with the second power. For the tower, span-wise mass and stiffness properties were scaled up in the same manner as the blade properties.

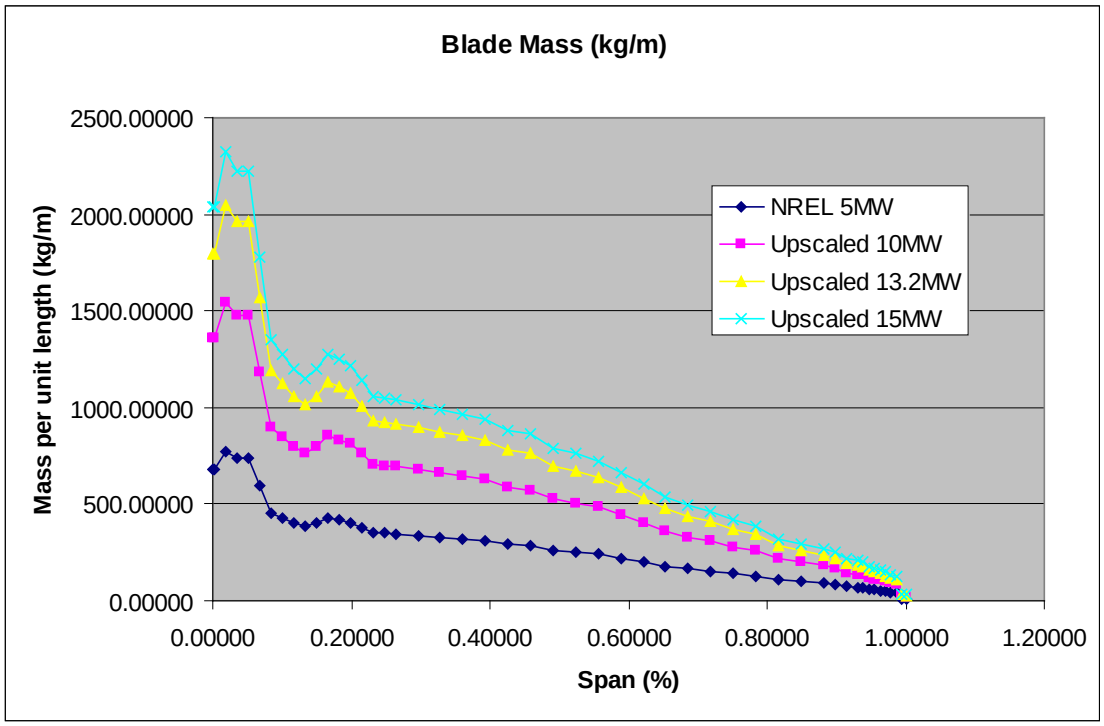

Figure 2. Scaled Blade Mass Per Unit Length

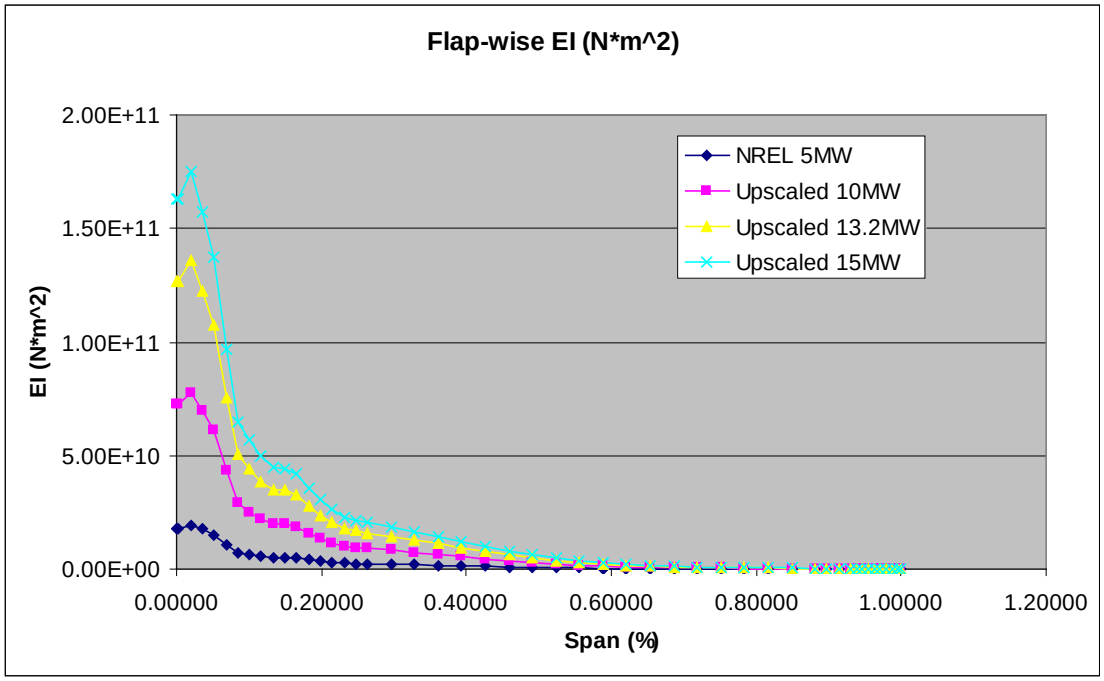

Figure 3. Scaled Blade Flap-wise Bending Stiffness

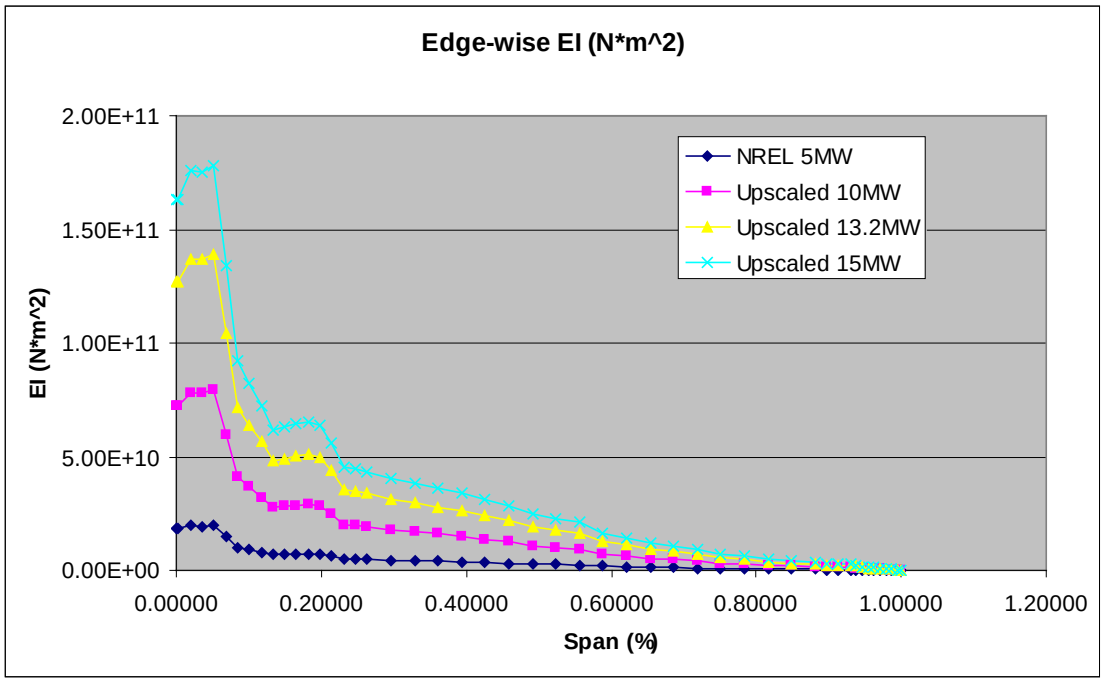

Figure 4. Scaled Blade Edge-wise Bending Stiffness

Table 3 lists general turbine and blade parameters for the upscaled models. Mass properties of the nacelle, drive train components, and tower height were also scaled. Mass was scaled with the third power while mass moments of inertia were scaled with the fourth power of the scale factor. Tables 4 and 5 list the mass properties of various turbine components.

Table 3. Scaled Turbine Properties

Machine Size	Rotor Diameter (m)	Blade Length (m)	Blade CG Location (m)	Blade Mass (kg)	Max Operating Speed (RPM)
5 MW	126	61.5	20.5	17740	12.1
10 MW	178.2	87.0	29.0	50184	8.56
13.2 MW	205	100.0	33.4	76402	7.44
15 MW	218.2	106.5	35.6	92131	6.99

Table 4. Scaled Turbine Nacelle Properties

Machine Size	Top Tower Mass (kg)	Hub Height (m)	Top Tower Inertia side-side (kg-m^2)	Top Tower Inertia fore-aft (kg-m^2)	Top Tower Inertia torsion (kg-m^2)
5 MW	350,000	90.0	3.500E+07	3.500E+07	2.608E+06
10 MW	990,101	127.3	1.400E+08	1.400E+08	1.043E+07
13.2 MW	1,507,363	146.4	2.452E+08	2.452E+08	1.827E+07
15 MW	1,817,693	155.9	3.148E+08	3.148E+08	2.345E+07

Table 5. Scaled Turbine Miscellaneous Properties

Machine Size	Nacelle Mass (kg)	Hub Mass (kg)	Nacelle Yaw Inertia (kg-m^2)	Generator inertia about HSS (kg-m^2)	Hub Inertia about rotor axis (kg-m^2)
5 MW	2.40E+05	5.68E+04	2.61E+06	534.116	1.16E+05
10 MW	6.79E+05	1.61E+05	1.04E+07	2.14E+03	4.64E+05
13.2 MW	1.03E+06	2.45E+05	1.83E+07	3.74E+03	8.12E+05
15 MW	1.25E+06	2.95E+05	2.35E+07	4.80E+03	1.04E+06

Further, it was assumed that the speed on the high speed shaft (HSS) was constant during up-scaling. This was accomplished with reducing the rotor speed by adjusting the gear box ratio to maintain a constant maximum tip speed.

2.2.3 SNL Targeted Layup: Initial 100-m Blade Definition

After completion of the scaling studies, EI and GJ properties of the 13.2 MW model (with 100-m blade) were used to start the detailed design of the blade itself. As stated previously, no composite layup data was provided in the NREL/DOWEC blade reports. However, the available structural and geometric data was deemed useful for scaling to 100-m blade length followed by creation of a "targeted" layup with closely matching properties to establish an initial 100-m blade design. Of course, many different layups along with different material choices can produce the same set of span-wise bending stiffnesses. In determining the layup, the process involved creation of a realistic, manufacturable layup while closely matching the targeted span-wise properties of the scaled-up 100-m blade. With the scaled external geometry from DOWEC (see Section 2.1) as a starting point, design details were considered and developed for shear web and spar cap placement, panel thickness, and material usage. Also, trailing and leading edge reinforcements were considered for the anticipated increased load-carrying capacity needed in these areas. The root build-up was designed for acceptance of large root bolts. The laminate thickness was then transitioned from the root circle to the airfoil at the maximum chord location.

Elliptical cross-sections were chosen to approximate the transition shapes between the root circle and the maximum chord airfoil. A two shear web design was chosen, and fiberglass with epoxy resin were the primary composite materials used throughout the blade. In this initial two shear web design, the shear webs were positioned to minimize the length of the unsupported aft panel near maximum chord. The forward shear web was placed near the maximum thickness of the airfoil along the entire span. The aft shear web was placed closer to the trailing edge. The spar cap width was tapered going outboard along the span resulting in a "box beam" type construction. It was decided to make the panel sections close to the same thickness as the spar cap to avoid large thickness drops about the circumference of the cross section. The spar cap thickness was designed to have diminishing thickness (ply dropping) from maximum chord and outboard along the span. The thickness of the spar cap principally affects the section flap-wise stiffness. Trailing edge and leading edge reinforcements were incorporated to improve edge-wise stiffness, which resulted in a thinner spar cap with their flap-wise contributions. The trailing edge and leading edge reinforcements were also designed with ply drops, and the thickness at each span-wise location was the same in both the trailing edge and leading edge areas. Also, the layup was designed to be symmetric with the same thicknesses on both the upper and lower blade surfaces in the leading edge, spar cap, panels, and trailing edge.

In Figure 5, the key elements in the design of a cross section are shown. Balsa core materials were used in the fore and aft panels as well as the shear webs (this was changed to foam core in the detailed design of the 100-m baseline – see section 4.0). The leading edge and trailing edge utilize reinforced laminates with no core. The spar cap is a thick reinforced laminate, primarily comprised of unidirectional materials.

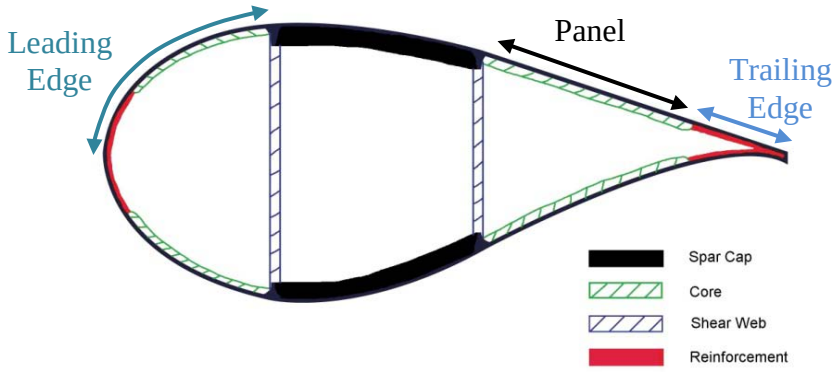

Figure 5. Representative Airfoil Cross Section with Two Shear Webs

A cross-sectional analysis code (PreComp [12]) was used to determine the laminate thicknesses at each station to closely match bending stiffnesses while considering the imposed constraints (e.g. web placement, ply drops, etc.). During the course of this work, an error was discovered in the PreComp code [13]. All calculations in this report, which utilized the PreComp code, were performed using the corrected version of the code. After performing the calculations, it was found that it is possible to design an all-glass layup for a 100-meter blade with realistic manufacturing considerations and blade weight to match the scaled-up bending stiffnesses. However, the laminate design was not evaluated for strength or for buckling resistance of the two shear web design. These evaluations were performed for the final baseline design discussed in Section 4.0.

Table 6 lists the resulting section properties for two span-wise locations – near maximum chord (19.8% span) and at an outboard span-wise location (68.6% span). Table 7 lists pertinent laminate data for these cross sections (excludes double-bias and random mat). No effort was made to also match the torsional and axial stiffnesses. "LE" refers to the part of the cross section from the leading edge to the forward shear web (see Figure 5). "Spar Cap" refers to layup between the two shear webs. "Panel" refers to the part of the cross section from the aft shear web to the beginning of the trailing edge reinforcement. "TE" reinforcement is the part of the cross section from termination of the panel to the trailing edge. The following were chosen for the entire blade span: 0.6 mm gelcoat over the entire external surface, 0.4 mm chopped mat and 1.2 mm of double bias material over entire blade internal and external surfaces. Note that the mass is lower for the Sandia Targeted Layup which could be due to efficiency in using trailing edge and leading edge reinforcements, missing parasitic mass or different material choices. However, again, no loads calculations were performed for this design.

Table 6. Section Properties Comparison between Upscaled NREL/DOWEC and Sandia Targeted Layup

Model	Span (%)	Airfoil (t/c)	Section Mass (kg/m)	Flap-wise EI (N-m^2)	Edge-wise EI (N-m^2)	Torsion, GJ (N-m^2)	Axial, EA (N)
Scaled NREL/DOWEC	19.8%	40.5%	1.08E+03	2.37E+10	4.96E+10	3.84E+09	1.08E+10
SNL Targeted Layup	19.8%	40.5%	*1.00E+03*	*2.39E+10*	*4.99E+10*	*2.18E+09*	*1.67E+10*
Percent Difference			*-7.4%*	*0.8%*	*0.6%*	*-43%*	*55%*
Scaled NREL/DOWEC	68.6%	21%	4.37E+02	8.83E+08	8.29E+09	1.46E+08	1.41E+09
SNL Targeted Layup	68.6%	21%	*3.13E+02*	*8.85E+08*	*8.32E+09*	*1.95E+08*	*5.16E+09*
Percent Difference			*-28%*	*0.2%*	*0.4%*	*34%*	*266%*

Table 7. Layup Information for SNL Targeted Layup

	Uni Material Thickness					Balsa Thickness (mm)
Station	**LE (mm)**	**Spar Cap (mm)**	**Panel (mm)**	**TE (mm)**		**LE, Panel, and TE**
19.8%	20	39	0	20		50
68.6%	9.5	16.5	0	9.5		10

2.2.4 UpWind 5 MW Composite Layup Up-scaling

While the up-scaled bending stiffnesses from the 5 MW properties provide a targeted set of properties for which to design a layup, we also performed upscaling of the 5 MW layup from the UpWind study to provide additional information for the 100-m baseline blade definition. A different approach was required when scaling up the UpWind material layup. Here, material thicknesses for each layer were scaled linearly along with the chord distribution as reported by DOWEC. The scaled material layup was then input to PreComp to compute the blade span-wise distribution of mass and stiffness properties using the material properties reported by UpWind. These equivalent beam properties could then be incorporated into a full system dynamics model. The UpWind based blade models were incorporated into the NREL turbine model by replacing the NREL/DOWEC based blade models.

In Figures 6 through 8, comparisons of the properties of the NREL/DOWEC 5 MW blades and those from cross-sectional analysis of the UpWind blade are plotted. Blade data for the UpWind 5 MW blade properties are only plotted for span-wise locations with DOWEC airfoil definitions; therefore, no transition data between the root and maximum chord are plotted.

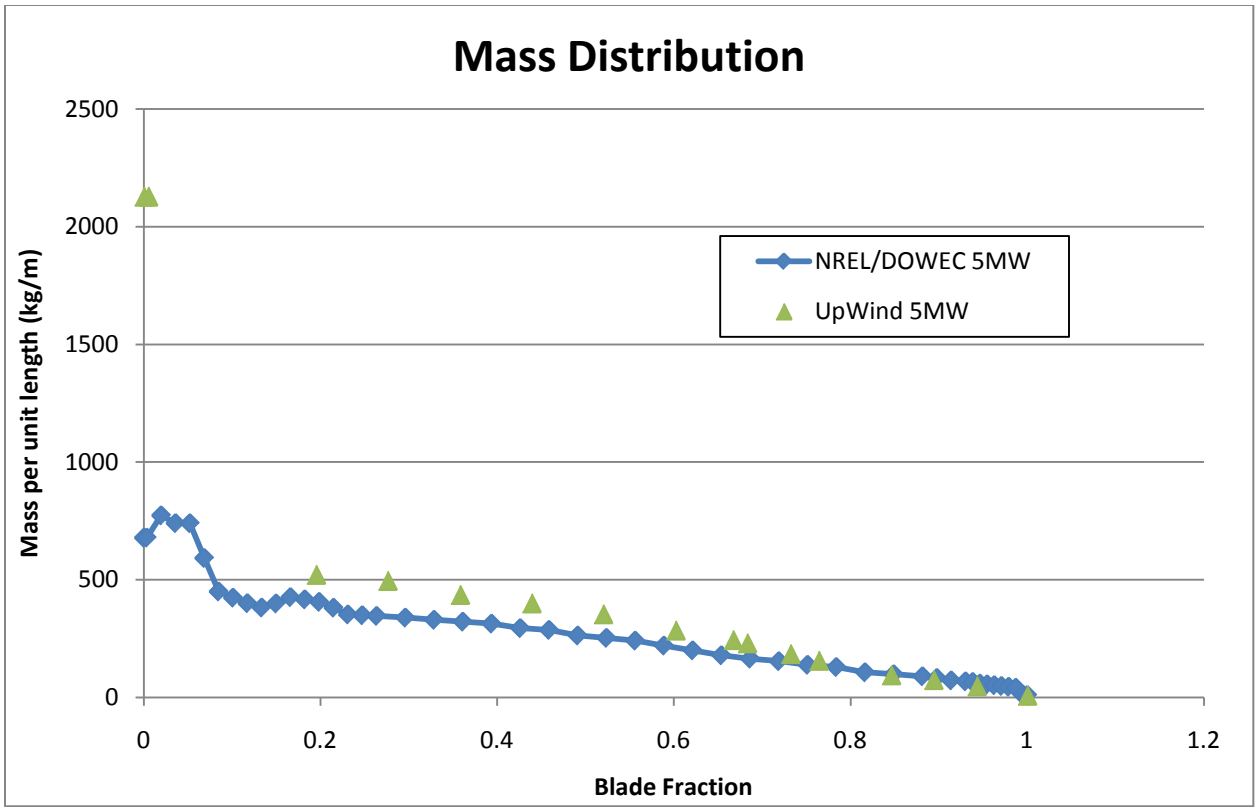

Figure 6. Mass Distribution for NREL/DOWEC and UpWind 5 MW Blades

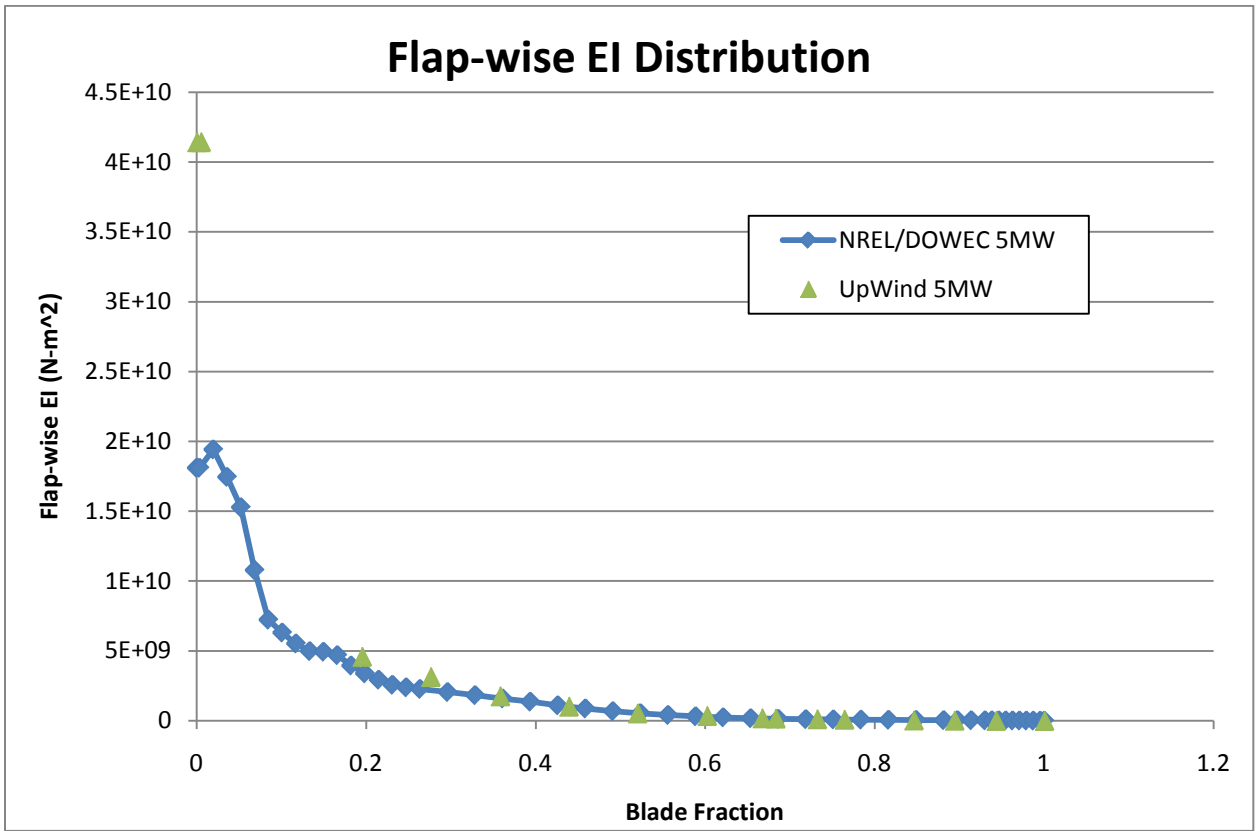

Figure 7. Flap-wise Stiffness Distribution for NREL/DOWEC and UpWind 5 MW Blades

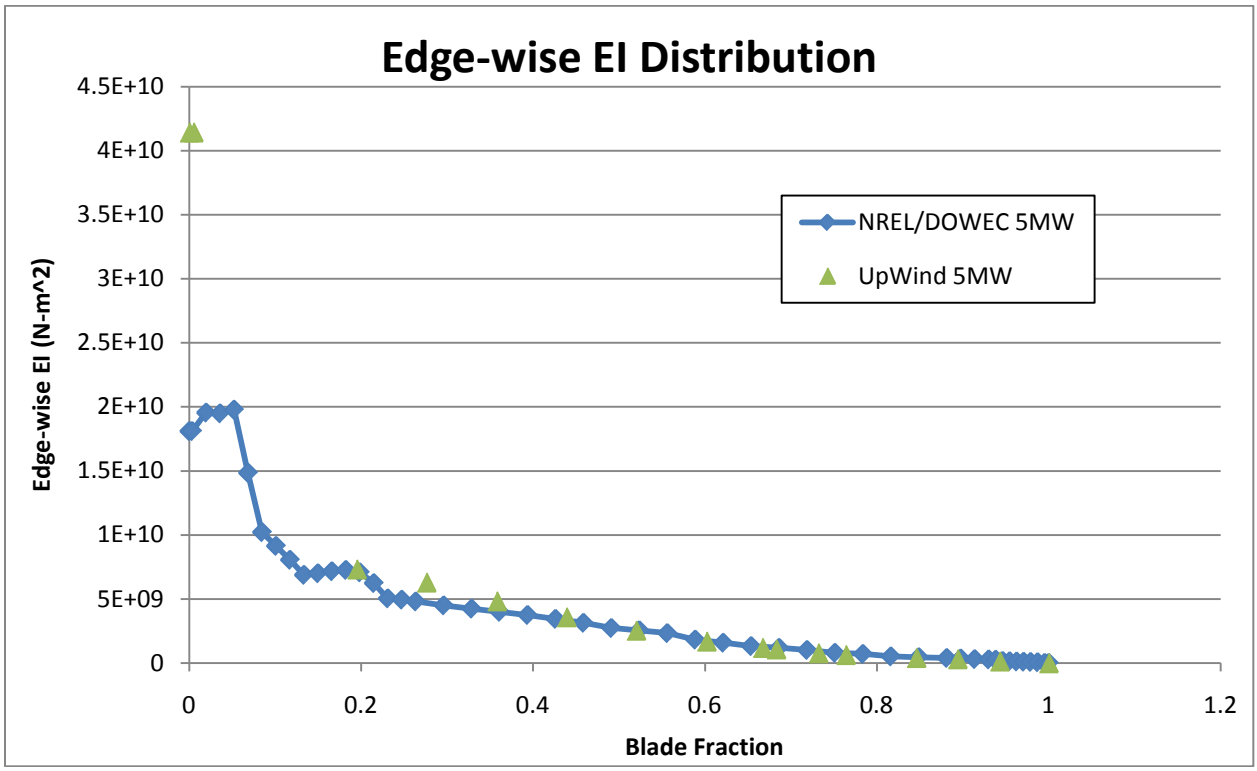

Figure 8. Edge-wise Stiffness Distribution for NREL/DOWEC and UpWind 5 MW Blades

2.2.5 Comparison of Blade Data from the DOWEC and UpWind Studies

From the preceding plots, observations can be made about the available blade models. First, the UpWind blade is noticeably heavier than the NREL/DOWEC blade, in particular at the root and inboard. The flap-wise and edge-wise bending stiffness values are in relatively good agreement with the exception of at the root. Although the DOWEC study was used in the development of both models, the selection of materials and material placement are apparently different.

In evaluating the available blade data from DOWEC, NREL, and UpWind, numerous important design details were not reported which are needed to define a detailed model. In developing the Sandia 100-meter All-glass Baseline Wind Turbine Blade, the following information was developed: (1) transition airfoils between the root circle and maximum chord airfoil, (2) root build-up, (3) shear web design, (4) layup manufacturability considerations, (5) detailed layup definition and materials selection, and (6) design loads analysis based on international design standards.

The SNL Targeted Layup provided very important information in further development of the 100-m baseline blade concept. The work provided good estimates of the laminate thicknesses needed in cross section design for conventional all-glass materials, and provided an early indication of the contribution of leading and trailing edge reinforcements to bending stiffnesses. Further, preliminary mass estimates were obtained.

2.3 Description of Turbine Controller Scaling

In order to simulate turbine operation in various wind conditions, pitch, yaw, and variable speed (VS) controllers are needed. The baseline controller in these studies is that developed for the NREL 5 MW turbine model [8]. For controlling larger turbines, the NREL controller was modified by adjusting maximum torque and maximum power settings for regulation at the desired values for the larger turbine. Actuation rates were kept constant by assuming that actuator force capability can be up-scaled appropriately. For example, the maximum pitch rate is assumed to be the same in our 13.2 MW turbine studies as that defined in the NREL 5 MW controller. Larger blades will require larger control effort. It is not clear if reasonably sized control actuators can be developed to maintain control authority while constraining the increase in actuator mass and size. This is an open question for research, and should be investigated in future studies.

3.0 Analysis of Up-scaled Models

The analysis performed to evaluate the 13.2 MW turbine models based on NREL/DOWEC and UpWind blades is presented in this section. First, the subset of IEC design load conditions considered as bounding cases is listed. Then, Germanischer Lloyd (GL) partial safety factors for materials and loads are listed along with the combined partial safety factors used to evaluate (1) ultimate strength, (2) tip deflection, (3) fatigue, and (4) bucking stability. Full system dynamics calculations using FAST were performed to determine structural response to design load conditions for the up-scaled full-turbine models (13.2 MW) based on the NREL/DOWEC blade and the UpWind blade. These results were then used to guide the design of the Sandia 100-m All-glass Baseline Blade described in Section 4.0.

3.1 Load Cases and Partial Safety Factors for Analysis

Table 8 lists the design load cases (DLC) selected for analysis of the 13.2 MW turbine models with respect to ultimate strength and deflection. These are based on the guidelines in IEC standards [14]. All load cases and scenarios required for certification are not exercised; however, those expected to create the largest loads are considered as bounding cases and are listed in Table 8. A Class IB site is chosen for siting of the turbine, which is considered to be a conservative choice with potential for offshore siting. The program IECWind [15] was used to generate the transient wind condition files needed for the FAST calculations.

Table 8. IEC Design Load Cases for Ultimate Strength and Deflection Analysis

Wind Condition	Description	IEC DLC Number	Design Situation (Normal or Abnormal)
ETM (Vin < Vhub < Vout)	Extreme Turbulence Model	1.3	Power Production (N)
ECD (Vhub = Vr +/- 2 m/s)	Extreme Coherent Gust with Direction Change	1.4	Power Production (N)
EWS (Vin < Vhub < Vout)	Extreme Wind Shear	1.5	Power Production (N)
EOG (Vhub = Vr +/- 2 m/s)	Extreme Operating Gust	3.2	Start up (N)
EDC (Vhub = Vr +/- 2 m/s)	Extreme Wind Direction Change	3.3	Start up (N)
EWM (50-year occurrence)	Extreme Wind Speed Model	6.2	Parked (A)
EWM (1-year occurrence)	Extreme Wind Speed Model	6.3	Parked (N)

GL partial safety factors for ultimate strength, fatigue, stability (buckling), and tip deflection calculations are listed in Tables 9-12 [16]. Further descriptions are found in Ref. 16. Table 9 lists the GL partial safety factors of materials for strength calculations.

Table 9. Strength Analysis Material Partial Safety Factors

Factors C_{ia}	Symbol	Value
Influence of aging	C_{1a}	1.35
Temperature effect	C_{2a}	1.1
Laminates made of prepregs, winding techniques, pultrusion or resin infusion method	C_{3a}	1.1
Wet laminate with hand lay-up, pressing techniques		1.2
Post-cured laminate	C_{4a}	1.0
Non post-cured laminate		1.1

The partial safety factors for all design drivers (ultimate strength, fatigue, etc.) are derived from a formula of the form

$$\gamma_{Mx} = \gamma_{M0} \prod_i C_{ix}$$

where $\gamma_{M0} = 1.35$ for all analyses, and C_{ix} are reduction factors dependent on, principally, the method of fabrication and material types.

For strength analysis, $\gamma_{Mx} = 1.35\big((1.35)(1.1)(1.1)(1.0)\big) = 2.205$ and includes the effects of aging and temperature, automated layup, and a post-cured laminate chosen from Table 9.

Table 10 lists the material GL partial safety factors for fatigue calculations.

Table 10. Fatigue Analysis Material Partial Safety Factors

Factors C_{ib}	Symbol	Value
Curve of high-cycle fatigue for the load cycle number N and slope parameter m	C_{1b}	$N^{1/m}$
Temperature effect	C_{2b}	1.1
UD reinforcements	C_{3b}	1.0
Non-woven fabrics and UD woven rovings		1.1
Woven fabrics and mats		1.2
Post-cured laminate	C_{4b}	1.0
Non post-cured laminate		1.1
For blade trailing edge	C_{5b}	1.0 to 1.2

For fatigue analysis, $\gamma_{Mx} = 1.35\big((1.0)(1.1)(1.1)(1.0)(1.0)\big) = 1.634$ based on Table 10.

Table 11 lists the GL partial safety factors for materials when performing stability/buckling calculations.

Table 11. Stability Analysis Material Partial Safety Factors

Factors C_{ic}	Symbol	Value
For massive laminates and skin layers of sandwich structures	C_{1c}	1.1
For core materials		1.3
For core materials, if verified minimum characteristics are used		1.0
Temperature effect	C_{2c}	1.1
Linear FEM		1.25
Non-linear FEM		1.0

For stability analyses, the combined partial safety factor for materials is different for skin and core materials. For skin materials, $\gamma_{Mx} = 1.35\big((1.1)(1.1)(1.25)\big) = 2.042$ based on Table 11, assuming a linear finite element analysis. This can be reduced if a nonlinear finite element calculation is used. For core materials, $\gamma_{Mx} = 1.35\big((1.0)(1.1)(1.25)\big) = 1.856$ assuming minimum characteristics are verified by testing and the use of a linear buckling calculation.

A summary of the partial safety factors for loads and the combined partial safety factors used in these analyses are listed in Table 12. In essence, the loads and materials factors combine, and a total safety factor has been computed. Depending on whether the load is normal (N) or abnormal (A), the loads factor is 1.35 or 1.1 respectively for ultimate strength.

Table 12. GL Partial Safety Factors

	Ultimate Strength	**Deflection**	**Fatigue**	**Stability (linear FEM)**
Loads	1.35/1.1	1.0	1.0	1.0
Materials	2.205	Not Applicable	1.634	Skin: 2.042 Core: 1.856
Combined (Loads and Materials)	2.977/2.426	Defined by % Clearance	1.634	Skin: 2.042 Core: 1.856

The deflection analysis is principally concerned with blade/tower strike. The GL standard describes the minimum allowed clearance, as a percentage of the clearance in the unloaded state for operating and parked rotor conditions. The standard states that a dynamic or aeroelastic analysis shall be performed.

For a turning rotor, a 30% minimum clearance is allowed while a 5% minimum clearance is allowed for a parked rotor. Based on upscaling from the NREL 5MW turbine, an overhang of 8.16 meters is determined. A tower radius of 2.0 meters is assumed. Shaft tilt and blade pre-cone angles of 5.0 and 2.5 degrees have been assumed in the turbine model. Shaft tilt of 5.0 degrees provides 8.93 meters of clearance while shaft tilt and precone combined provide 13.38 meters of clearance. These calculations use the rotor radius of 102.5 meters in their calculation.

The total clearance is determined by the sum of the overhang and shaft tilt/precone contributions minus the tower radius, and is computed to be 19.54 meters. For a dynamic or aeroelastic calculation with a turning rotor, 13.67 meter tip deflection is allowed. For the parked rotor, 18.56 meters is allowed.

3.2 Design Loads Analysis Results of 13.2 MW Turbine Models

Aeroelastic simulation results for two 13.2 MW turbines are presented; the first case is with the upscaled NREL/DOWEC blade and the second case with the upscaled UpWind blade. We assess these blades with respect to the previously listed design load cases which help us guide the development of the Sandia 100-m All-glass Baseline Blade. In the final sub-section, trends with blade length scale are discussed.

3.2.1 13.2 MW Turbine Analysis (with NREL 5 MW Blade as Baseline)

The NREL 5MW FAST model was scaled to a 13.2 MW turbine giving a 100 meter blade length (205 m rotor diameter). A number of design load cases, as noted earlier in Table 8, were developed, run, and analyzed. These were the most severe (all extreme) loading cases. A summary of the results for peak root bending moments (flap-wise and edge-wise) and peak tip deflection are listed in Table 13. For the 50-year and 1-year extreme wind condition (EWM50 and EWM01, respectively), the turbine was parked with a zero degree pitch angle (i.e. flat to the wind). Note that the largest flap-wise root bending moment occurs for the EWM50 condition while the largest edge-wise root bending moment occurs for the extreme horizontal wind shear (EWSH) condition at rated speed (although a number of the operating load cases produce similarly valued edge-wise root bending moments). The largest tip deflection results from the EWM50 load case. Maximum tip deflections for all load cases are less than the allowables, which are described above.

Results for the normal wind profile at rated (NWPR) are also tabulated for comparison. The normal wind profile is a constant wind speed case with a rated wind speed of 11.3 m/sec. Maximum rotation rate is 7.44 rpm.

Table 13. 13.2 MW (with NREL/DOWEC 5 MW Baseline) Root Bending Moments and Tip Deflection for Selected Design Loads

Machine	IEC DLC Number	Load Case	Flap-wise	Edge-wise	Tip Defl
			(kN-m)	(kN-m)	(m)
13.2 MW	1.4	ECD+R	62,600	38,000	12.3
13.2 MW	1.4	ECD-R	64,200	38,000	13.4
13.2 MW		NWPR	43,100	38,400	8.7
13.2 MW	6.2	EWM50 (0^o pitch)	101,800	16,140	14.7
13.2 MW	6.3	EWM01 (0^o pitch)	67,860	10,600	9.8
13.2 MW	1.5	EWSV+R	48,560	37,990	9.9
13.2 MW	1.5	EWSH-R	50,720	38,750	10.1
13.2 MW	3.2	EOGR	50,690	37,990	9.4
13.2 MW	3.3	EDC-R	44,600	38,320	9.1
13.2 MW	1.3	ETM-R	28,770	32,510	5.8

Based on the computed moments, strain was computed using Bernoulli beam theory with the formula

$$\varepsilon = \frac{Mc}{EI}$$

where the bending moment M is computed in FAST and the bending stiffness EI is defined along the span. The distance c was chosen to be the distance from the neutral axis to the blade outer surface for flap calculations. This distance was chosen to be that from the pitch axis to the trailing edge for edge-wise strain calculations as it was assumed maximum strain would occur at the trailing edge.

In addition to the root strains, strains were computed at several points along the blade span (23%, 50%, and 76%) which corresponded to aerodynamic nodes in the FAST model. The peak flap-wise and edge-wise strains at 23% span are listed in Table 14. The peak flap-wise strain is 4104 micro-strain for the 50-year extreme wind condition (EWM50), while the peak edge-wise strain is 2665 micro-strain for an extreme coherent gust with direction change at rated (ECD+R). We compare these results to those of the NREL 5MW for the same wind conditions and find 4379 micro-strain (flap-wise, EWM50). The flap-wise strains due to aerodynamic loads should remain unchanged based on scaling laws, and this appears to be the case here although a small numerical discrepancy exists. Also, for the NREL 5MW model, we find a peak edge-wise strain of 989 micro-strain (ECD+R). The edge-wise strain at 23% span has nearly tripled for the up-scaled 100-m blade from the 61.5 meter blade as noted in Table 14. We expect that the edge-wise strains will increase for the longer blade due to the growing blade weight; however, this result shows increase in strain greater than the expected scaling. The results in Table 14 also demonstrate the difference in the effect of scale for operating versus non-operating cases as the strains are nearly unchanged from 5 to 13.2 MW for the parked EWM50 case, while the strains grow for the operating ECD+R case with larger gravitational loads. It is noted here that although the largest bending moments occur at the root, the largest strains occur near maximum chord (approx 20% of span).

Table 14. 13.2 MW (with NREL/DOWEC 5 MW Baseline) Peak Strains at 23% Span

Machine	Load Case	Flap-wise	Edge-wise
		Micro-strain	Micro-strain
5 MW	*ECD+R*	*3443*	*989*
13.2 MW	ECD+R	2874	2665
5 MW	*EWM50(0^o pitch)*	*4379*	*794*
13.2 MW	EWM50(0^o pitch)	4104	615

From Table 15 we see that the root flap-wise strains are similar for both the 5MW and 13.2MW sized machines. This is expected from scaling laws presented in Section 2.0. However, edge-wise strains grow for the operating cases (ECD+R and NWPR) for the longer blade length at a rate slightly higher than the expected linear growth rate.

Table 15. 13.2 MW (with NREL/DOWEC 5 MW Baseline) Peak Strains at the Root (0% span)

Machine	Load Case	Flap-wise	Edge-wise
		Micro-strain	Micro-strain
5 MW	*ECD+R*	*1604*	*487*
13.2 MW	ECD+R	1410	856
5 MW	*EWM50(0^o pitch)*	*2390*	*338*
13.2 MW	EWM50(0^o pitch)	2294	364
5 MW	*NWPR*	*1036*	*483*
13.2 MW	NWPR	971	865

3.2.2 13.2 MW Turbine Analysis (with UpWind 5 MW as Baseline)

The span-wise properties derived from cross-sectional analysis of the scaled 100-m UpWind blade layup were incorporated into the 13.2 MW FAST aero-elastic model. Only the blade models were changed from the model analyzed in the previous section. All other turbine parameters were the same. The same load cases were then simulated for the 13.2 MW turbine with the 100-m up-scaled UpWind blades. Root bending moments for the most severe load cases identified in analysis of the 13.2 MW (NREL/DOWEC based) turbine were calculated and are listed in Table 16. The maximum flap-wise root bending moment was found to be 107,700 kN-m (EWM50), while the peak edge-wise root bending moment was found to be 39,760 kN-m (ECD+R). The edge-wise root bending moment for ECD+R increased by 4.6% from the NREL/DOWEC based 13.2 MW model due to the larger weight of the UpWind blade (90, 608 kg versus 76,356 kg) and the small increase in CG location (33.3 meters versus 33.7 meters). For EWM50, the tip deflection is 14.3 meters and for ECD+R it is 13.0 meters.

Table 16. 13.2 MW (with UpWind 5 MW Baseline) Root Bending Moments and Tip Deflections for Selected Design Loads

Machine	Load Case	Flap-wise	Edge-wise	Tip Defl
		(kN-m)	(kN-m)	(m)
13.2 MW	ECD+R	70,560	39,760	13.0
13.2 MW	EWM50 (0^o pitch)	107,700	16,530	14.3

Additionally, we note the maximum strain at 23% span which is tabulated in Table 17. For the parked turbine, the flap-wise strains are the dominant design driver. However, for an operating turbine

with a 100-meter blade, the edge-wise strain near the maximum chord is nearly equal to the flap-wise strain (Table 17).

Table 17. 13.2 MW (with UpWind 5 MW Baseline) Peak Strains at 23% Span

Machine	Load Case	Flap-wise	Edge-wise
		Micro-strain	Micro-strain
13.2 MW	ECD+R	2088	1985
13.2 MW	EWM50 (0^o pitch)	2941	1056

3.3 Summary of Analysis: Effect of Scale and Trends with Blade Length

An early indication from these scaling studies is that a blade requires additional edge-wise reinforcement as blade length increases beyond 61.5 meters. At this point, fatigue and buckling trends have not been addressed, but are addressed in the final design – see Section 4. Further, we observe that the length of the unsupported blade panels are growing and buckling may require further attention. It is not known if either the NREL/DOWEC or UpWind 61.5 meter blades were designed to satisfy buckling or fatigue requirements, although they satisfy strain and deflection allowables for extreme loads. The analysis in the previous sections indicates that flap-wise strain is nearly independent of scale based on aeroelastic simulations for operating and parked cases. However, the edge-wise strains have grown significantly for the 13.2 MW rotor compared to the 5 MW rotor for operating cases. Maximum deflections are within allowables for the load cases considered.

4.0 Sandia 100-m Baseline Blade Design and Structural Analysis

4.1 Design Considerations

Considerations for the design of a blade cross section include the number and location of shear webs, spar dimensions, utilization of leading edge and/or trailing edge reinforcements, skin and core thickness, materials and airfoil thickness ratio. These choices are dictated by loads and resulting strains, and aerodynamic design in the case of t/c ratio and twist. The chord schedule is an important consideration which impacts both aerodynamic and structural design, although it is mostly dictated by aerodynamic requirements.

In the initial design phase, a two shear web design was pursued for the Sandia 100-m All-glass Baseline Wind Turbine Blade as this has been the typical design choice for state of the art of large blades. The design approach began by considering a typical, representative blade cross section such as shown in Figure 9. At each station along the span of the blade, the layup design considered material choice and thickness of four regions of the station: (1) spar cap, (2) core panels, (3) shear webs, and (4) leading and trailing edge reinforcements. The layups were designed initially using information gained from the scaling studies discussed in the previous sections.

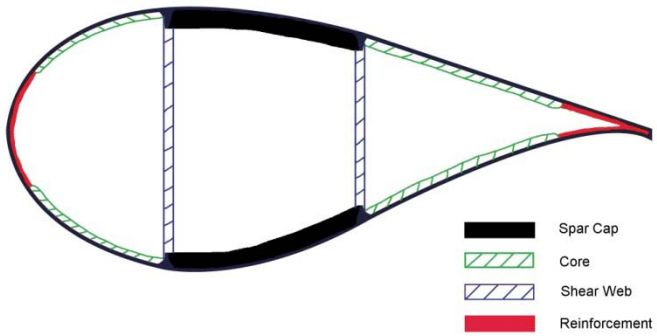

Figure 9. Representative Airfoil Cross Section with Two Shear Webs

Modifications to the model included the addition of weight for extra resin that is typical in traditional manufacturing processes. While extra adhesive from excessive bond line thickness was not explicitly captured, the added extra resin included all the parasitic mass. During fabrication extra resin may be supplied to the mold to ensure that fibers are properly wetted. Extra resin is also likely absorbed into core materials (especially foam core).

Constraints were placed on spanwise thickness transitions of laminates to ensure realistic manufacturability of the layup design. For example, the spar cap and trailing edge reinforcement laminate thicknesses were constrained such that they began with a single layer inboard, transitioned to a larger thickness outboard and then tapered down to a single layer close to the tip.

4.2 Initial Design Results and Observations

For the analyses of the initial 100-m baseline layup design, tip deflection and span-wise strains were calculated for the all-glass, two shear web design. The results demonstrated that tip deflection and strains (strength) were within specifications considering design standard safety factors for materials and

loads. At this point in the design, a high-fidelity finite element model was created using the Sandia NuMAD blade modeling code [17]. This model was used to perform buckling calculations.

For the linear buckling analysis, loads were applied in the flap-wise direction corresponding to the EWM50 condition at zero degree pitch angle. This condition corresponds to IEC DLC 6.2, which is an abnormal condition with electrical grid power loss. It is assumed this is a worst case with no ability to pitch the blades out of the wind. The initial model failed to satisfy the design buckling loads with safety factors as the aft panel demonstrated buckling modes near maximum chord and outboard of maximum chord along the trailing edge. Aft panels were then stiffened by increasing the foam panel thickness and by adding additional layers of uni-axial materials. Although the buckling criterion was satisfied after a few design iterations, it was determined that the final blade weight was unrealistically high. In this initial two shear web design, the shear webs were positioned to minimize the length of the unsupported aft panel near maximum chord. The forward shear web was placed near the maximum thickness of the airfoil along the entire span. One consideration for the aft shear web location was to place it at a constant distance from the forward shear web. This would have resulted in a constant width spar cap. However, buckling was a concern; therefore, the aft shear web was placed such that near maximum chord it was closer to the trailing edge. As a result, the shear web separation distance was tapered from a maximum value at the 2% span-wise location to a minimum value outboard at 94% span. Nonetheless, this choice to place the aft shear web toward the trailing edge to minimize the unsupported aft panel size near maximum chord did not provide a suitable design solution to satisfy the buckling requirement.

It was decided that a better design solution included the addition of a third shear web. A “short” web beginning inboard of maximum chord and running just beyond midspan was added. As a result, the two principal shear webs could be located at a constant separation distance providing a constant width, “box beam” spar construction. From a manufacturing point of view, this is an improvement over the tapered-width spar cap approach. And, it was expected that the third web would enable satisfaction of the buckling criterion while reducing blade weight.

The subsequent sections provide the detailed design geometry and layup information for the final design satisfying strength, tip deflection, buckling, and fatigue criterion. In this design, only glass materials with foam core materials were considered. Again, a three shear web design was selected for the final design.

4.3 Sandia 100-m Baseline Blade Geometry

The external geometry of the Sandia 100-m Baseline Blade uses scaled-up chord and airfoil definitions from the DOWEC study. The detailed chord distribution used in this study is provided in publicly available reports [5,6]; however, limited airfoil definitions were included. Transition airfoil specifications between the root circle and maximum chord were not documented in the DOWEC report. Therefore, required transition airfoil shapes were generated by interpolation resulting in a gradual transition from the maximum chord airfoil to an elliptical shape and finally to a circle at the root. Span-wise blade thicknesses (i.e. thickness to chord ratios) were transitioned by smoothing the maximum thickness of the cross sections along the span to avoid significant surface concavity or dimpled regions susceptible to buckling or stress concentrations. With this designed thickness distribution, thickness to chord ratios for the span-wise airfoils were computed. The addition of the transition airfoils permitted cross sectional analysis of the composite layup in the transition region. This was a purely geometric interpolation. No consideration was given to aerodynamic properties at this stage of the blade

development. Also, a few outboard airfoils were scaled about the chord line to ensure a smooth blade thickness along the entire span. Further, the DOWEC-defined chord schedule was modified at the blade tip to transition the chord length to a near point at the tip.

Airfoil designations and chord schedule for the Sandia 100-meter All-glass Baseline Wind Turbine Blade are listed in Table 18 along with blade twist and pitch axis offset of the leading edge. A plot of the airfoils for the transition region is provided in Figure 10, and the outboard airfoils are plotted in Figure 11. Plots of the planform and thickness distribution are shown in Figures 12 and 13. Note that in order to smooth the blade thickness distribution, it was necessary to make adjustments to the thickness to chord of several airfoil shapes. The t/c ratios for the blade stations are listed in parentheses with the airfoil descriptions in Table 18. The new airfoils were computed by scaling airfoil geometry about the chord line. This was deemed acceptable for this structural analysis although thickening/thinning of the airfoil should be about the camber line for aerodynamic considerations.

Table 18. Sandia 100-m Baseline Blade Airfoil and Chord Properties
Note: Thickness to chord ratio in parentheses for transition and modified outboard airfoils

Station Number	Blade Fraction	Chord (m)	Twist (deg)	Pitch Axis (Fraction)	Airfoil Description
1	0.000	5.694	13.308	0.500	Cylinder
2	0.005	5.694	13.308	0.500	Cylinder
3	0.007	5.694	13.308	0.500	Transition (99.25%)
4	0.009	5.694	13.308	0.500	Transition (98.5%)
5	0.011	5.694	13.308	0.500	Transition (97.75%)
6	0.013	5.694	13.308	0.500	Ellipse (97%)
7	0.024	5.792	13.308	0.499	Ellipse (93.1%)
8	0.026	5.811	13.308	0.498	Ellipse (92.5%)
9	0.047	6.058	13.308	0.483	Transition (84%)
10	0.068	6.304	13.308	0.468	Transition (76%)
11	0.089	6.551	13.308	0.453	Transition (68%)
12	0.114	6.835	13.308	0.435	Transition (60%)
13	0.146	7.215	13.308	0.410	Transition (51%)
14	0.163	7.404	13.177	0.400	Transition (47%)
15	0.179	7.552	13.046	0.390	Transition (43.5%)
16	0.195	7.628	12.915	0.380	DU99-W-405
17	0.222	7.585	12.133	0.378	DU99-W-405 (38%)
18	0.249	7.488	11.350	0.377	DU99-W-350 (36%)
19	0.276	7.347	10.568	0.375	DU99-W-350 (34%)
20	0.358	6.923	9.166	0.375	DU97-W-300
21	0.439	6.429	7.688	0.375	DU91-W2-250 (26%)
22	0.520	5.915	6.180	0.375	DU93-W-210 (23%)
23	0.602	5.417	4.743	0.375	DU93-W-210
24	0.667	5.019	3.633	0.375	NACA-64-618 (19%)
25	0.683	4.920	3.383	0.375	NACA-64-618 (18.5%)
26	0.732	4.621	2.735	0.375	NACA-64-618
27	0.764	4.422	2.348	0.375	NACA-64-618
28	0.846	3.925	1.380	0.375	NACA-64-618
29	0.894	3.619	0.799	0.375	NACA-64-618
30	0.943	2.824	0.280	0.375	NACA-64-618
31	0.957	2.375	0.210	0.375	NACA-64-618
32	0.972	1.836	0.140	0.375	NACA-64-618
33	0.986	1.208	0.070	0.375	NACA-64-618
34	1.000	0.100	0.000	0.375	NACA-64-618

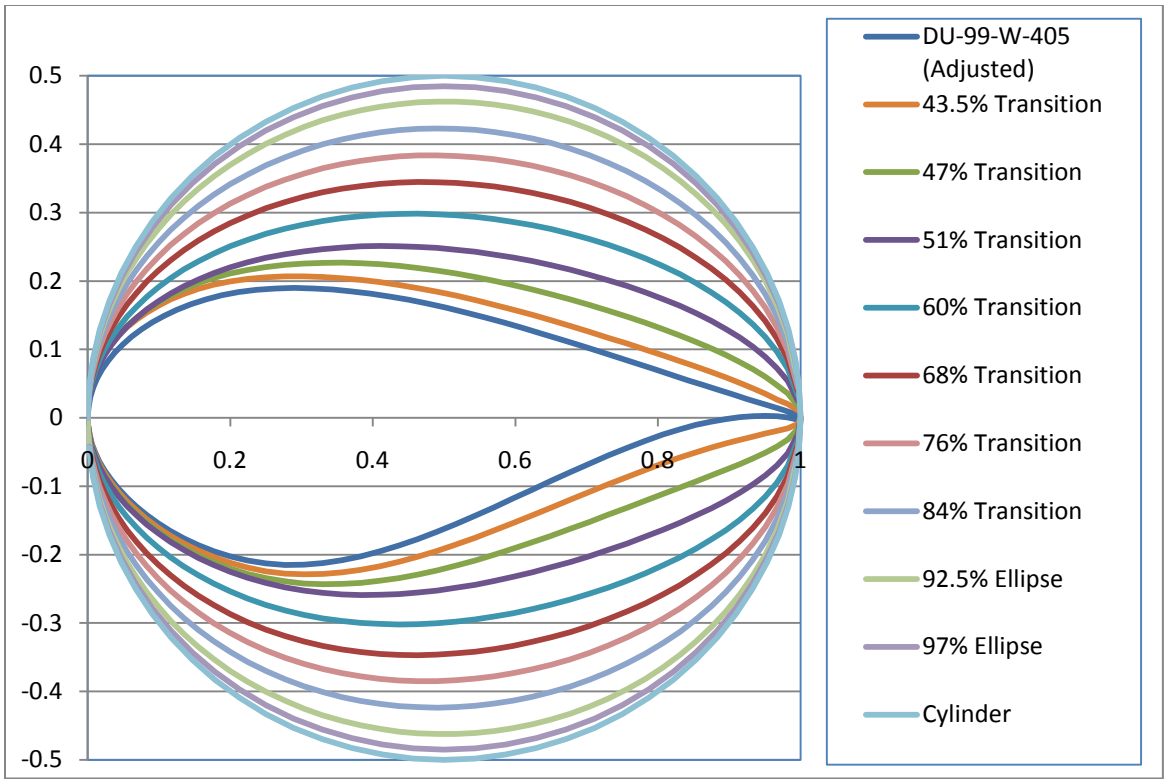

Figure 10. Transition Airfoil Geometries for the Sandia 100-m Baseline Blade

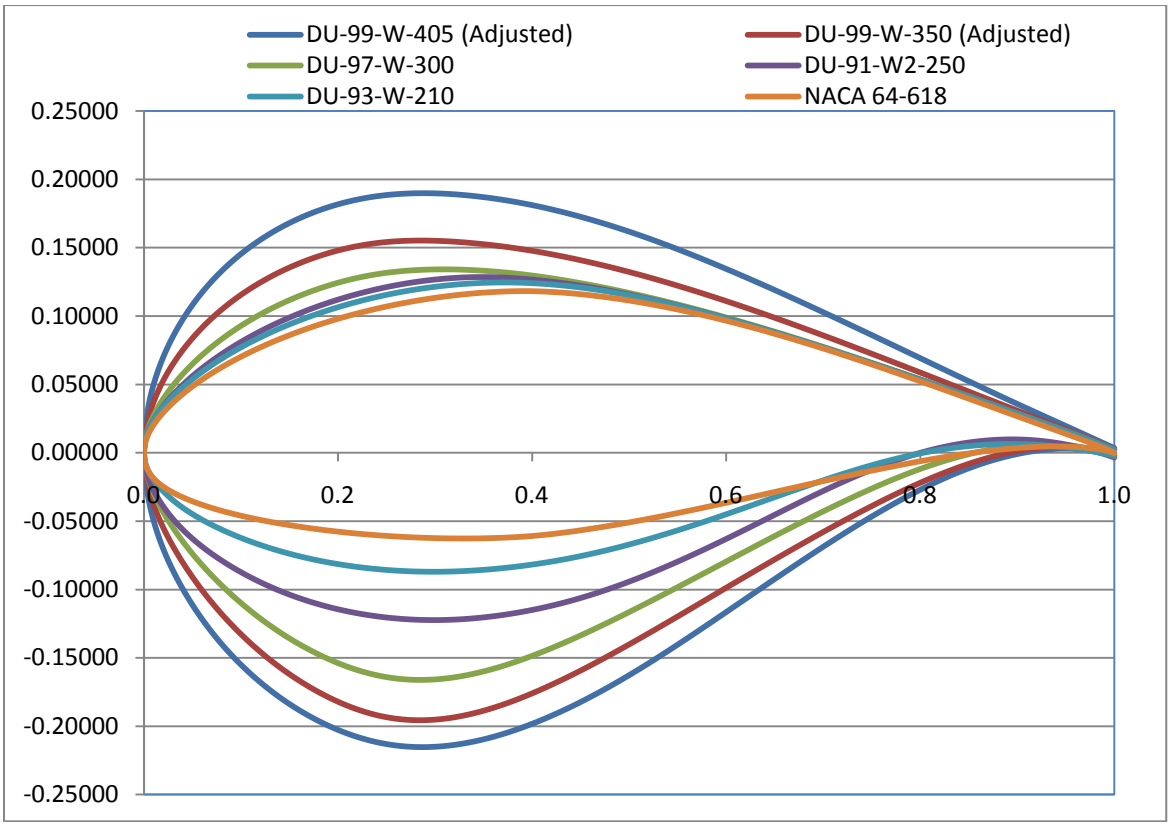

Figure 11. Outboard Airfoil Geometries for the Sandia 100-m Baseline Blade

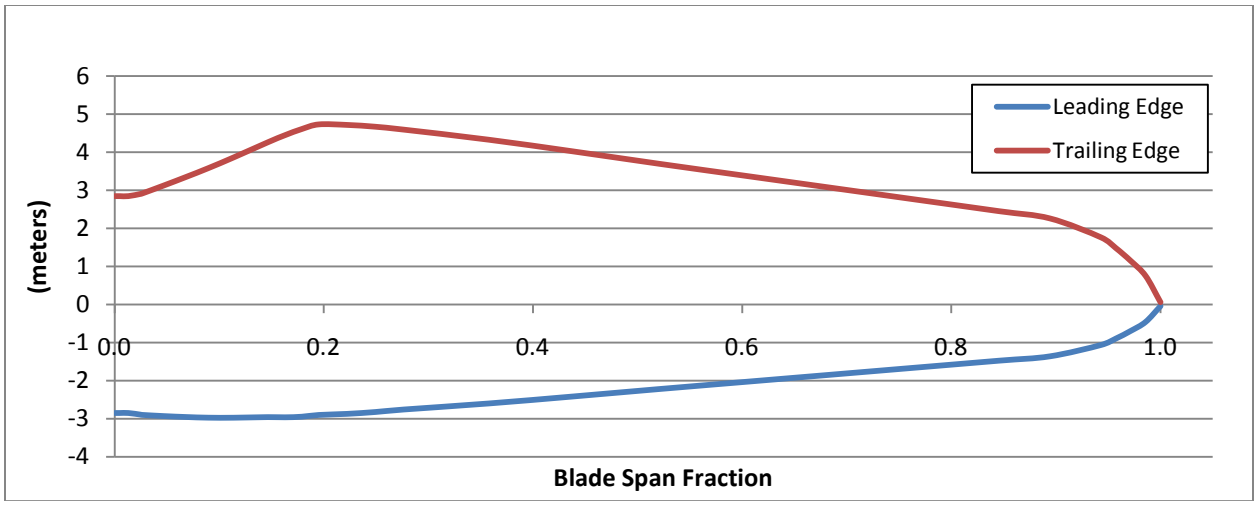

Figure 12. Sandia 100-m Baseline Blade Planform

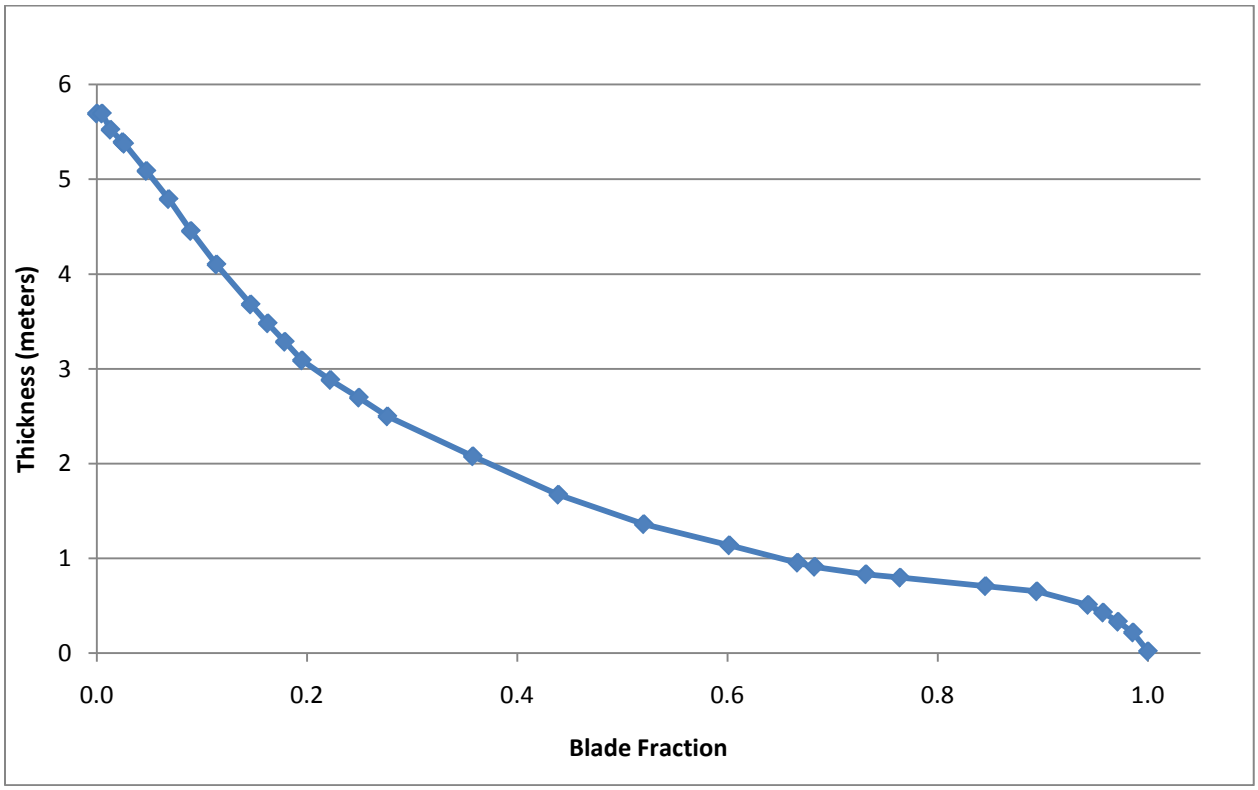

Figure 13. Sandia 100-m Baseline Blade Thickness Distribution at Maximum Thickness

Figure 14 provides three views of the blade surface geometry: flap-wise, edge-wise, and isometric.

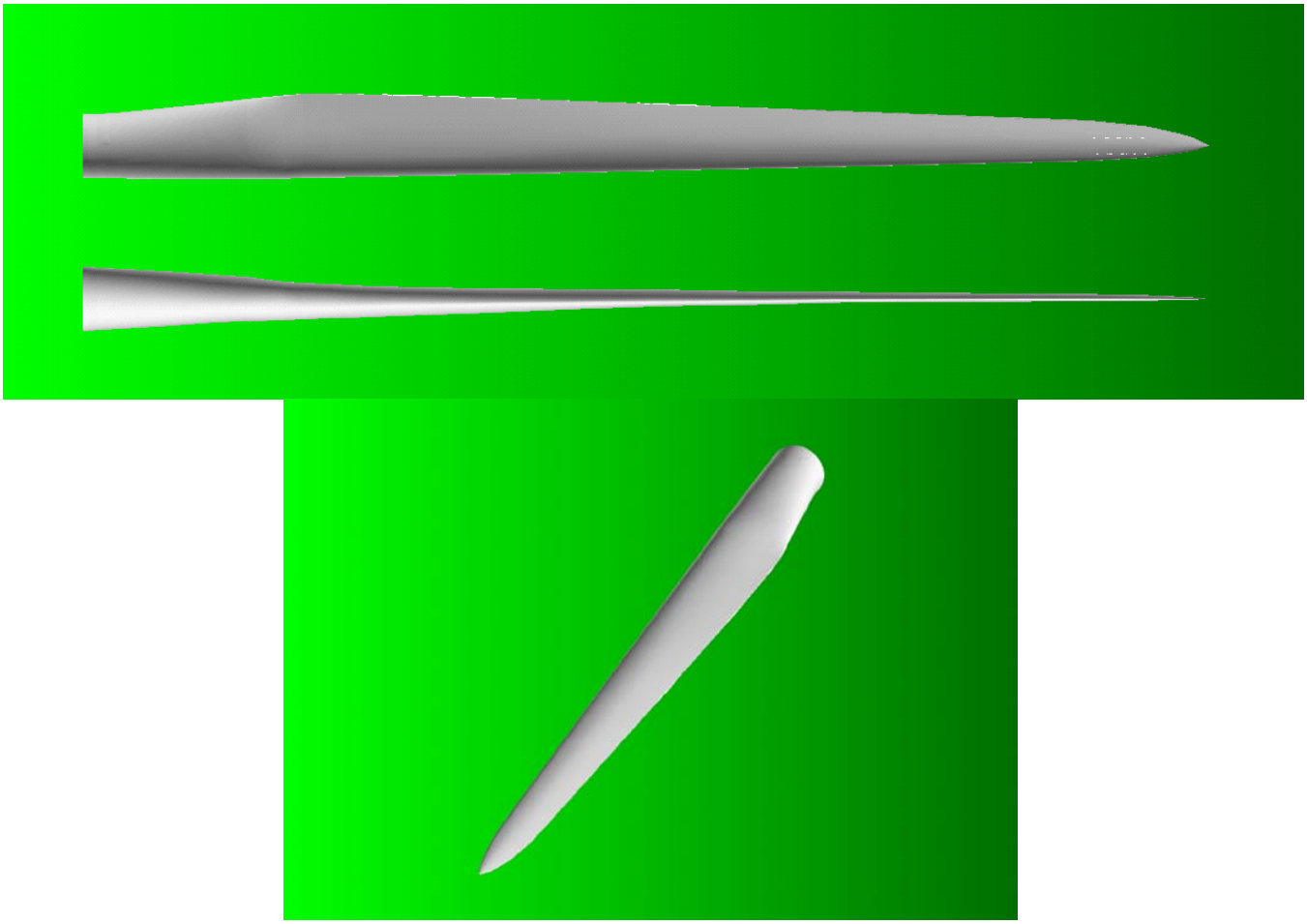

Figure 14. Views of Blade Surface Geometry

4.4 Sandia 100-m Baseline Blade Layup Definition

Table 19 lists the elastic and ultimate strength material property data for the laminates chosen for this design. These are glass fabrics and epoxy resin materials, which were selected from the DOE/MSU Composite Material Fatigue Database [18]. E-LT-5500 was chosen for the uni-directional material, and Saertex was chosen for the double bias material. Epoxy resin (EP-3) was selected as the matrix material. The ultimate strength properties are 95/95 fits to multiple single cycle failure data points in tension and compression [18] for the uni-axial E-LT-5500/EP-3 laminate and are mean data for the Saertex/EP-3 double bias laminate. Based on the volume fractions indicated in Table 19, the mass density of the E-LT-5500 uni-directional laminate is 1920 kg/m^3 and the mass density for the Saertex-based double bias laminate is 1780 kg/m^3. Properties for the triaxial material, which we denote as SNL Triax, were determined by averaging the test-derived data for the uni-axial and double bias material. Fatigue properties for a laminate consisting of uni-axial and double bias materials were derived from the Database and are listed along with the fatigue analysis results in a later section (See Appendix A.).

Table 19. Material Property Data Selected from DOE/MSU Database

Laminate Definition			**Longitudinal Direction**								**Shear**
			Elastic Constants				**Tension**		**Compression**		
VARTM Fabric/resin	**lay-up**	**V_F %**	**E_L GPa**	**E_T GPa**	**υ_{LT}**	**G_{LT} GPa**	**UTS_L MPa**	**ε_{max} %**	**UCS_L MPa**	**ε_{min} %**	**τ_{TU} MPa**
E-LT-5500/EP-3	$[0]_2$	54	41.8	14.0	0.28	2.63	972	2.44	-702	-1.53	30
Saertex/EP-3	$[\pm45]_4$	44	13.6	13.3	0.51	11.8	144	2.16	-213	-1.80	----
SNL Triax	$[\pm45]_2[0]_2$	---	27.7	13.65	0.39	7.2	----	----	----	----	----

E_L and E_T - Longitudinal & transverse modulii, υ_{LT} - Poisson's ratio, G_{LT} & τ_{TU} - Shear modulus and ultimate shear stress. UTS_L - Ultimate longitudinal tensile strength, ε_{MAX} - Ultimate tensile strain, UCS_L - Ultimate longitudinal compressive strength. ε_{MIN} - Ultimate compressive strain.

Based on the maximum strain data from tests and combined safety factors, +8,196 and -5,139 micro-strain allowables are determined for the uniaxial laminate by dividing the ultimate tensile and compressive strain values in Table 19 by a combined safety factor of 2.977. Computed in the same fashion, the allowables for the double bias laminate are computed to be +7,255 and -6,046 micro-strain in tension and compression, respectively. Of course, a comparison of the two materials is not equitable because the uni-axial material properties are 95/95 fits while the double bias material properties are from mean data. If additional testing was conducted on the double bias material, we would expect the allowable strain to be reduced by 10-15%.

In the previously discussed scaling studies, all strains were well below these allowable values. This means as we move into this baseline design it is also likely that strains will be below allowable maximum strains. A traditional design practice has included applying further "knock-down" factors to these allowable strains to account for fatigue and stability considerations; however, our approach involves performing the complete suite of analyses to verify that all design criteria are satisfied.

Table 20 lists additional materials used in this design. These include coating material, extra resin, and foam core material. The foam properties were chosen to correspond with those used in the UpWind layup [10].

Table 20. Material Properties for Additional Materials

Material	E_L GPa	E_T GPa	G_{LT} GPa	υ_{LT}	Density (kg/m^3)
GelCoat	3.44	3.44	1.38	0.3	1235
Resin	3.5	3.5	1.4	0.3	1100
Foam	0.256	0.256	0.022	0.3	200

Table 21 lists the laminate schedule for 34 stations along blade (which correspond to those in Table 18). This schedule is divided into the columns which define the laminate thickness (units of mm) for the root buildup and the four principal parts of the cross section (spar cap, trailing edge reinforcement, leading edge panels, and aft panels). Note that no extra uni-axial reinforcement was added to the leading edge. Figure 15 shows graphically the laminate placement and shear web locations for the data listed in Table 21. The trailing edge reinforcement is highlighted in orange. The spar cap placement is highlighted in blue. The two principal shear webs are located to the top and bottom sides of the spar cap. The third shear web location is shown by the red line in Figure 15. The leading edge panel is defined as the grey area between the leading edge and the beginning of the spar cap. The aft panel is defined as the grey area between the spar cap and trailing edge reinforcement. The third shear web resides within the aft panel region.

The root buildup is composed of triaxial material. As the root buildup tapers down in thickness, the spar cap begins to increase in thickness. The maximum thickness of the spar cap is 136 mm at maximum chord (19.5%) and it reaches a minimum thickness at 94.4% of span and continues close to the tip. Trailing edge reinforcement, which includes both uni-axial and foam materials, also begins near the root (0.5%) and continues to the tip. The trailing edge reinforcement is a constant width of 1.0 meters from its beginning until it reaches 94.4% span, at which it begins to taper to the tip. Foam was chosen for the panel core material, which is placed fore and aft of the spar cap (See Table 20 for its properties). Additional foam was placed in the aft panel from 4.7 to 16.3 meters to improve buckling resistance. The choice of adding foam thickness rather than adding additional uni-axial material for reinforcement was made to minimize weight. Both the low pressure and high pressure blade surfaces were designed with the same layup thicknesses. The spar cap has a constant width of 1.5 meters. Thus the two principal shear webs, which begin at 2.4 meters and terminate at 94.4 meters, are positioned 0.75 meters fore and aft of the pitch axis. The third shear web begins at 14.6 meters and ends at 60.2 meters, and is positioned at 78% of chord (as measured from leading edge to trailing edge) at the beginning and 68% of chord at its termination.

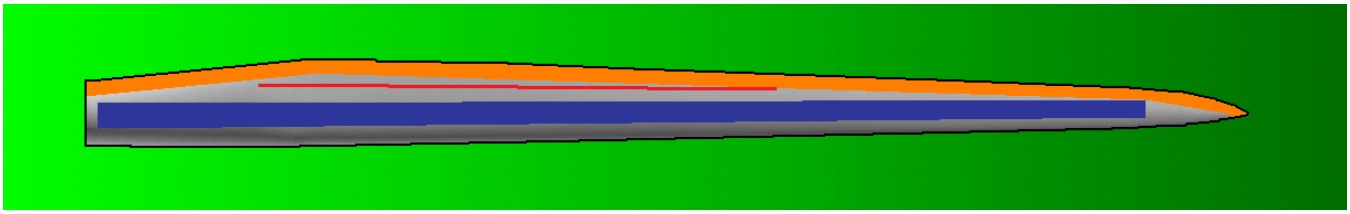

Figure 15. Planform of Sandia 100-m Baseline Blade with Laminate Designations (Blue: Spar Cap, Orange: trailing edge reinforcement, Red: Third Shear Web)

Table 21. Laminate Schedule for Sandia 100-m Baseline Blade (* indicates termination)

Station Number	Blade Span	Root Buildup	Spar Cap	TE Reinforcement	LE Panel	Aft Panel
		Triax/EP-3	E-LT-5500/EP-3	E-LT-5500/EP-3, Foam	Foam	Foam
	(-)	(mm)	(mm)	(mm)	(mm)	(mm)
1	0.000	160				
2	0.005	140	1	1		
3	0.007	120	2	2		
4	0.009	100	3	3		
5	0.011	80	4	5		
6	0.013	70	10	7	1	1
7	0.024	63	13	8	3.5	3.5
8	0.026	55	13	9	13	13
9	0.047	40	20	13, 0	30	100
10	0.068	25	30	18, 0	50	100
11	0.089	15	51	25, 60	60	100
12	0.114	5	68	33, 60	60	100
13	0.146	*	94	40, 60	60	100
14	0.163		111	50, 60	60	60
15	0.179		119	60, 60	60	60
16	0.195		136	60, 60	60	60
17	0.222		136	60, 60	60	60
18	0.249		136	60, 60	60	60
19	0.277		128	30, 40	60	60
20	0.358		119	30, 40	60	60
21	0.439		111	15, 20	60	60
22	0.521		102	8, 10	60	60
23	0.602		85	4, 10	60	60
24	0.667		68	4, 10	60	60
25	0.683		64	4, 10	55	55
26	0.732		47	4, 10	45	45
27	0.765		34	4, 10	30	30
28	0.846		17	4, 10	15	15
29	0.895		9	4, 10	10	10
30	0.944		5	4, 10	5	*
31	0.957		5	4, 10	5	
32	0.972		5	4, 10	5	
33	0.986		5	4, 10	5	
34	1.000		*	*	*	

In addition to the detailed span-wise layup data in Table 21, the entire blade internal and external surfaces have 5 mm of triaxial material. Extra mass is included by modeling 5 mm of epoxy resin on the internal blade surface. The external surface includes 0.6 mm of gelcoat. The extra epoxy resin and surface gelcoat are included to produce a more realistic blade design weight. All three shear webs

consisted of the same layup, 80 mm of foam sandwiched between 3 mm of double bias material (Saertex/EP-3) on the outer surfaces.

The spar cap width was determined by the distance between the two principal shear webs. The forward shear web was placed 0.75 meter fore of the pitch axis near the maximum thickness of the airfoils (approximately 30% chord), which improves the flap-wise stiffness. The aft shear web was placed, as previously mentioned, an equal distance aft of the pitch axis. A constant width spar cap is considered an advantage for manufacturing considerations, and was made possible by inclusion of the third shear web (see Figure 15 for its location).

For the six materials used in this design, which are listed in Tables 19 and 20, their contribution to the total blade weight was calculated using the PreComp code. These results are listed in Table 22, and provide a description of the placement of laminates/materials in the design along with total mass and percentage of total blade mass. The table shows that 42.8% of the blade weight is composed of uni-axial material laminates used in the spar caps and trailing edge reinforcements. The extra resin accounts for 6,863 kg of blade weight while the gelcoat accounts for 920 kg. In total, the inclusion of extra resin and gelcoat comprise 6.7% of the total blade weight. The shear webs were found to total 10,270 kg or 8.9% of the total blade weight.

A further analysis, separating the fiber and resin content, shows that 32.5 % of the blade weight (37,647 kg) is uni-axial fiberglass, 8.7% (10,045 kg) is double bias fiberglass, and the largest fraction of 44.7% (51,718 kg) is resin. This resin content includes resin used to construct the E-LT-5500/EP-3, SNL Triax, and Saertex/EP-3 laminates as well as extra resin noted in Table 22. The bill of materials summary is provided in Table 23.

Table 22. Materials Usage Summary for Sandia 100-m Baseline Blade

Laminate/Material	Usage/Location	Mass (kg)	Percent Blade Mass
E-LT-5500/EP-3	Spar caps, trailing edge reinforcement	49,527	42.8%
SNL Triax	Root build-up, internal & external surfaces	38,908	33.6%
Foam	Core panels, shear webs	15,333	13.3%
Extra Resin	extra weight (interior surface)	6,863	5.9%
Saertex/EP-3	Shear webs	4,112	3.6%
Gelcoat	Coating	920	0.8%

Table 23. Bill of Materials for Sandia 100-m Baseline Blade

Material	Description	Mass (kg)	Percent Blade Mass
E-LT-5500	Uni-axial Fiberglass	37,647	32.5%
Saertex	Double Bias Fiberglass	10,045	8.7%
EP-3	Resin	51,718	44.7%
Foam	Foam	15,333	13.3%
Gelcoat	Coating	920	0.8%

A selection of blade cross sections is plotted in Figure 16. The airfoil geometry is true in scale. Key sections are plotted in which shear webs begin and end. In several sections, beginning at 14.6 meters span, the nose and tail areas are plotted with thicknesses smaller than the actual thicknesses. This is a result of necessarily reducing the thickness of the shell elements at the nose and tail by a factor of 10 to avoid elements with large thickness to radius of curvature values and causing computational errors. The material properties of the modified elements are appropriately scaled up by a factor of 10. The plots demonstrate the relative thickness of the layup defined in Table 21 for the various locations about the circumference of the cross section. For example, at maximum chord (19.5 meters), the spar cap has thickness of 136 mm while the leading edge panel, which is defined from the leading edge to the forward shear web, has thickness of 60 mm. The aft panel has thickness of 60 mm, and is defined from the 2nd shear web to the beginning of the trailing edge reinforcement. The third (aft) shear web is just beyond the midpoint of the aft panel. The trailing edge reinforcement at maximum chord has thickness of 120 mm, which can also be viewed in Figure 16(e). Note that these thickness values describe only the materials listed in Table 21. Additional materials are present throughout the entire layup (i.e. 0.6 mm gelcoat coating, 5 mm SNL Triax on interior and exterior surfaces, and 5 mm resin on interior surface).

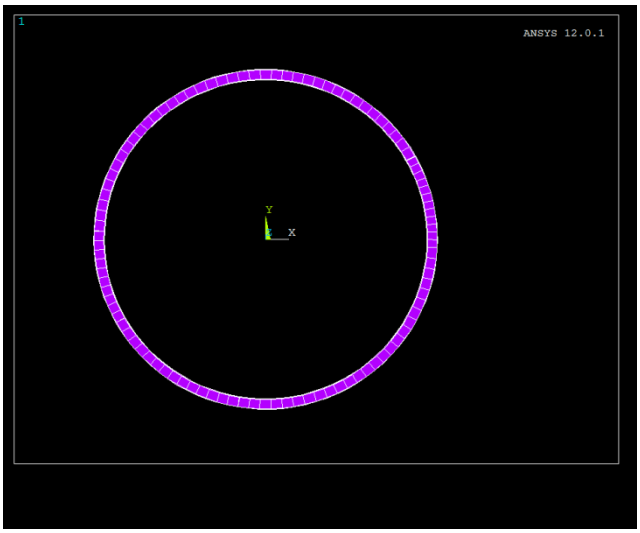

(a) 0.0 meters (root circle)

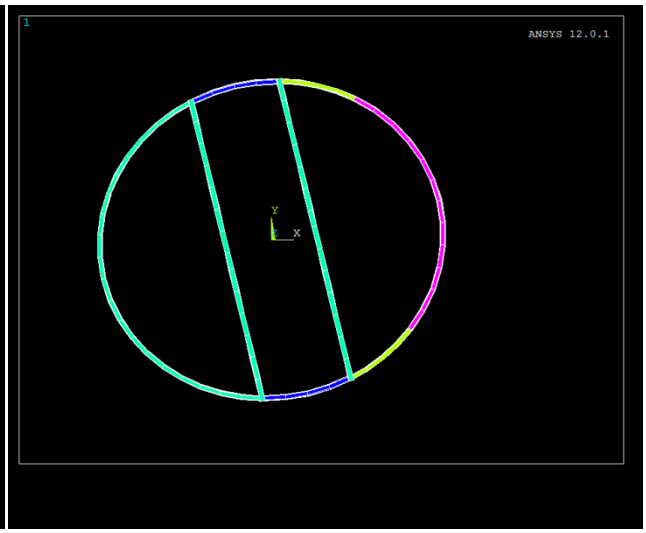

(b) 2.4 meters (principal shear webs begin)

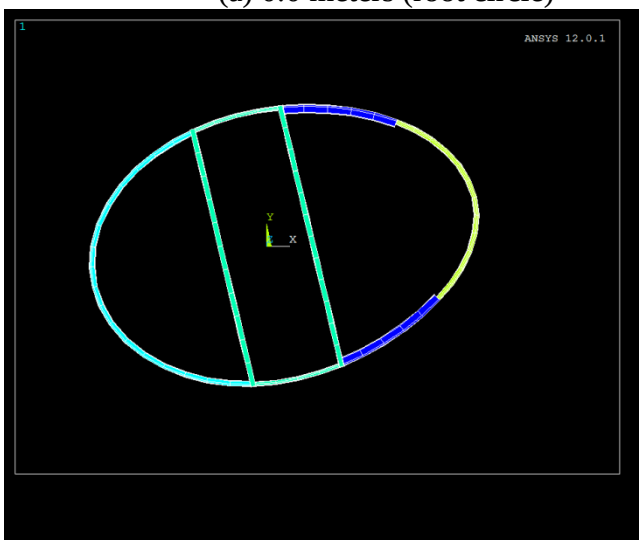

(c) 8.9 meters(transition)

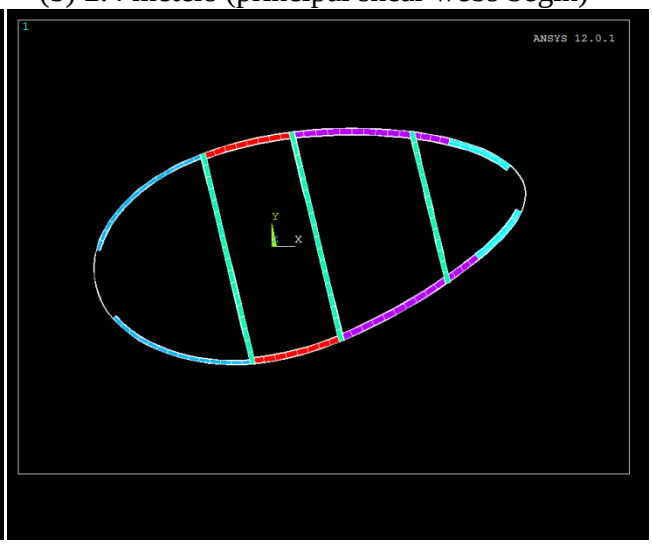

(d) 14.6 meters (third shear web begins)

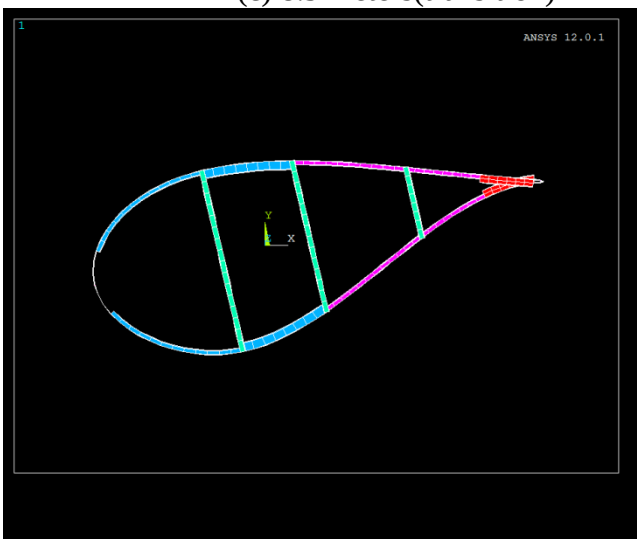

(e) 19.5 meters (maximum chord)

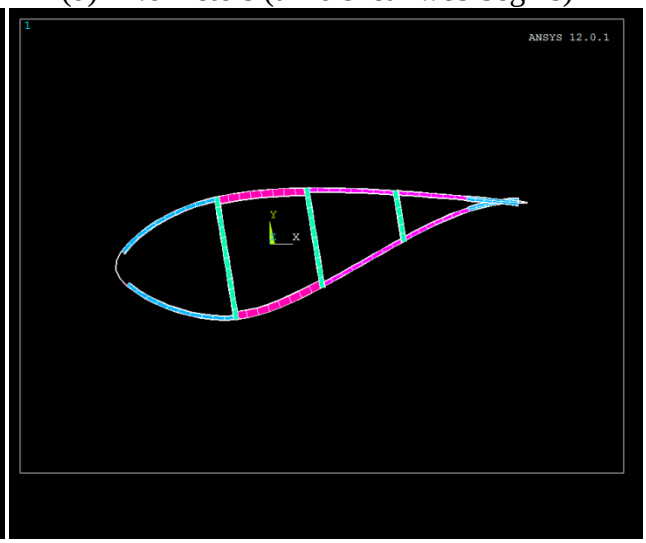

(f) 35.8 meters

Figure 16 (a through f). A Selection of Cross Sections along Sandia 100-m All-glass Baseline Blade Span (cont'd on next page)

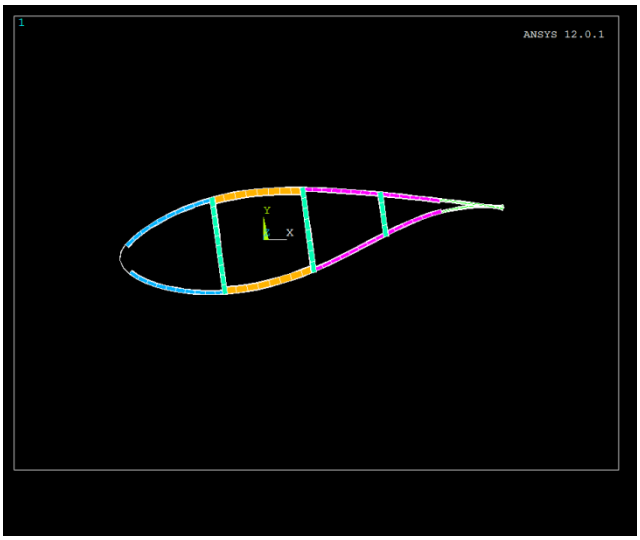

(g) 43.9 meters

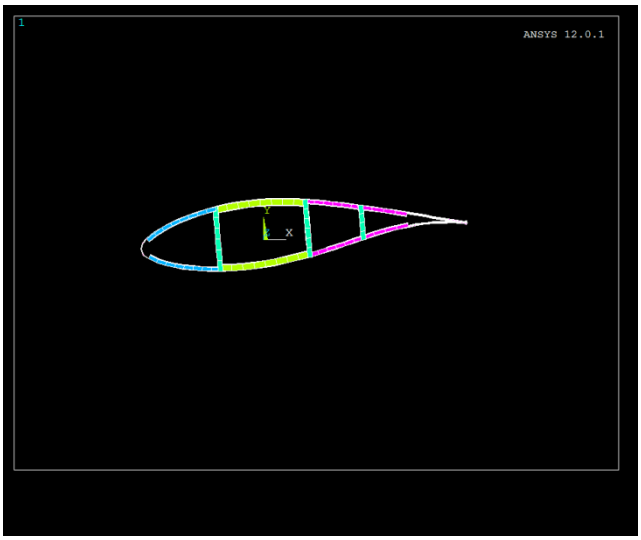

(h) 60.2 meters (third shear web ends)

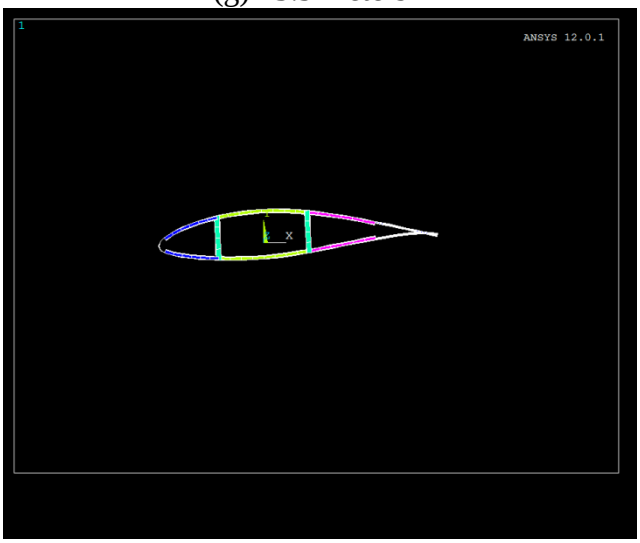

(i) 73.2 meters

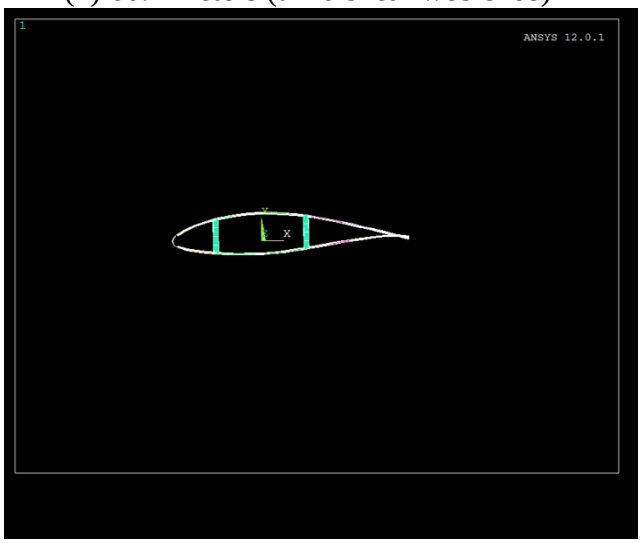

(j) 84.6 meters

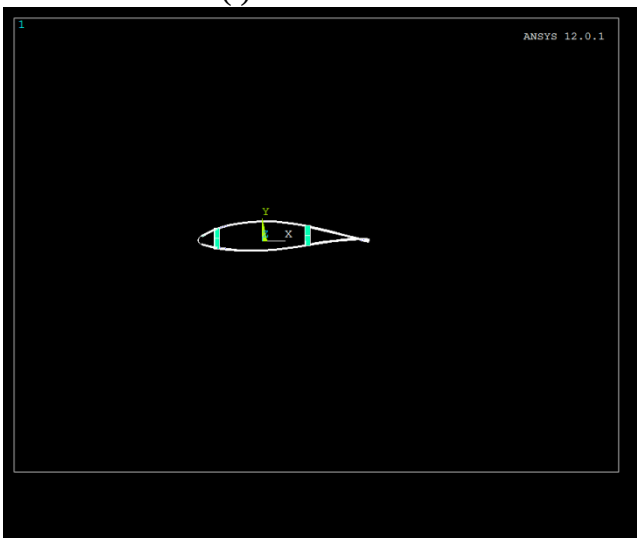

(k) 94.3 meters (principal shear webs end)

(l) 98.6 meters

Figure 16 (g through l). Continued: A Selection of Cross Sections along Sandia 100-m All-glass Baseline Blade Span

4.5 Sandia 100-m Baseline Blade Analysis Results

Some 13.2 MW baseline turbine design properties are listed in Table 24. The cut-in and cut-out wind speeds are 3 and 25 m/s. The maximum rotation rate of this variable speed machine is 7.44 rpm. We have chosen to perform the analysis with Class IB loads to not limit the potential siting of this turbine.

Table 24. General Turbine Properties

Property	Value
Rotor Radius/Hub Radius	102.5m/2.5m
Blade Mass	114,172 kg
Class	IB
Max Rotor Speed	7.44 RPM
Rated Wind Speed	11.3 m/s

The blade mass reported in Table 24 was calculated by the FAST program. A summation of the midpoint averaged beam mass properties from PreComp produced a mass estimate of 115,684 kg while the ANSYS finite element model produced a mass estimate of 118,634 kg. Based on the value reported in Table 24, and accounting for the extra mass attributed to the resin material modeled on the interior surface, the mass scaling factor of this design is 3.33 when compared to the UpWind (5MW) blade, which is also an all-glass layup design. A mass scaling factor of 3.0 is expected by conventional upscaling. However, the mass of the Sandia 100-meter All-glass Baseline Blade is higher than the conventional scaling trend. This can be understood by considering: (1) the need for additional reinforcements to satisfy buckling and fatigue life requirements, (2) the addition of a third shear web, (3) the use of all-glass materials, and (4) no systematic attempt to optimize the layup or shear web thickness for blade weight reduction.

4.5.1 Strain and Deflection Calculations

Bending moments and deflections were computed by running design load cases in the FAST code. Results for bounding case loads at the root are tabulated in Table 25.

Table 25. Sandia 100-m Baseline Blade Root Bending Moments and Tip Deflections for Selected Design Loads

Machine	Load Case	Flap-wise (kN-m)	Edge-wise (kN-m)	Tip Defl (m)
13.2 MW	ECD+R	67,410	47,220	10.1
13.2 MW	ECD-R	74,810	52,460	11.9
13.2 MW	NWPR	49,250	48,600	7.3
13.2 MW	EWM50 (0^o pitch)	110,700	17,300	12.3
13.2 MW	EWM01 (0^o pitch)	73,300	11,320	8.2
13.2 MW	EWSV+R	58,440	47,260	8.6
13.2 MW	EWSH-R	57,450	47,620	8.3
13.2 MW	ETM-R	37,410	45,930	5.4

As expected, the worst case flapwise load is the EWM50 at zero degree pitch angle. This is an abnormal condition which assumes loss of grid power and inability to pitch the blades out of the wind. It is interesting to note that the ECD-R condition produces the second highest flapwise loads on the blade and the highest edgewise. For ETM-R, the edge-wise moments (and strains) are higher than the

flap-wise moments (and strains) at the root. This would appear to have implications on fatigue life-time calculations and the potential for design of large blades to be driven by gravitational loads.

As described previously, the allowable tip deflection is calculated with assumed values for rotor overhang, shaft tilt angle, precone angle, and tower radius. These values were selected in these analyses to be 8.16 meters, 5.0 degrees, 2.5 degrees, and 2.0 meters, respectively. As a result, for operating cases the allowable tip deflection is 13.67 meters, which is greater than the largest operating case tip deflection of 11.9 meters (see ECD-R in Table 25). The allowable tip deflection for a parked rotor is 18.56 meters. For the EWM with 50-year occurrence, the computed tip deflection is well within this allowable. Although the EWM condition with 50-year occurrence produces the largest deflection, it is apparent that the operating condition of ECD-R is the driver for analysis of blade/tower clearance.

The blade root thickness was designed to be 160 mm (6.3 inch) thick in order to accept the anticipated large number/size of root bolts. The root thickness was chosen after reviewing root thickness for smaller machines, and considering upscaling to the equivalent 100-meter length. These calculations do not consider "knock-down" factors to account for the presence of the bolts. However, the root strains for the current analyses are small in comparison to allowable strains as shown in Table 26. Note: the root thickness may have to be increased depending on details of attachment at root.

Table 26. Sandia 100-m Baseline Blade Root (0% span) Strains for Selected Design Loads

Machine	Load Case	Flap-wise	Edge-wise
		(micro-strain)	(micro-strain)
13.2 MW	ECD+R	596	418
13.2 MW	ECD-R	661	464
13.2 MW	NWPR	435	430
13.2 MW	EWM50 (0^o pitch)	979	153
13.2 MW	EWM01 (0^o pitch)	648	100
13.2 MW	EWSV+R	517	418
13.2 MW	EWSH-R	508	421
13.2 MW	ETM-R	331	406

The strains at maximum chord (19.5% span) are found to be considerably higher than at the root (Table 27), although all are well below allowable strains. Allowable strains are described in Section 4.4.

Table 27. Sandia 100-m Baseline Blade Maximum Chord (19.5% span) Strains for Selected Design Loads

Machine	Load Case	Flap-wise	Edge-wise
		(micro-strain)	(micro-strain)
13.2 MW	ECD+R	1750	1214
13.2 MW	ECD-R	2253	1169
13.2 MW	NWPR	1487	862
13.2 MW	EWM50 (0^o pitch)	2662	300
13.2 MW	EWM01 (0^o pitch)	1770	202
13.2 MW	EWSV+R	1632	1169
13.2 MW	EWSH-R	1701	1150
13.2 MW	ETM-R	1071	1187

4.5.2 Buckling Evaluation

The initial layups were found to be acceptable with respect to allowable strain and tip deflection. However, they did not satisfy buckling requirements; therefore, additional reinforcements were designed into critical buckling areas in the aft panel and trailing edge region. The foam in the core panels was thickened, and extra foam and uni-axial material were added to the trailing edge region. Reinforcements were investigated along the entire blade span as additional reinforcements were also added at the tip (outboard of 94.4%) to prevent buckling. Also, the spar thickness was increased in a few critical areas to prevent buckling. These modifications resulted in the final design layup (Table 21). As a result, the ultimate strains and deflections were reduced significantly as shown in the previous section when compared to scaling studies results of Sections 3.2.1 and 3.2.2. The iterations required to improve the buckling resistance of the entire blade underlie the importance of a high-fidelity blade structural model in blade design. Further, the early indication that buckling is a significant design driver for very large blades indicates that validated structural models and accurate predictive structural analysis codes will be critical in producing very large blades with high reliability.

A high-fidelity ANSYS finite element blade model was created using the NuMAD code (Figure 17). Both buckling and detailed stress analyses were performed using ANSYS. A linear static analysis with prestress effects was performed with the EWM50 loads derived from a FAST analysis. The forces at the aerodynamic nodes of the FAST model were applied to nearby nodes in the FE model, flap-wise in the down-wind direction (Figure 18). The load was applied at 18 points along the blade span. An eigen buckling solution was then performed that considers the prestress effects of the linear static solution. Because the full load was applied statically, satisfaction of the buckling requirement is met when buckling mode frequencies are computed to be greater than the required safety factor. This is because the buckling frequencies are equal to the scaling factor of the applied static load at which a particular buckling mode will occur.

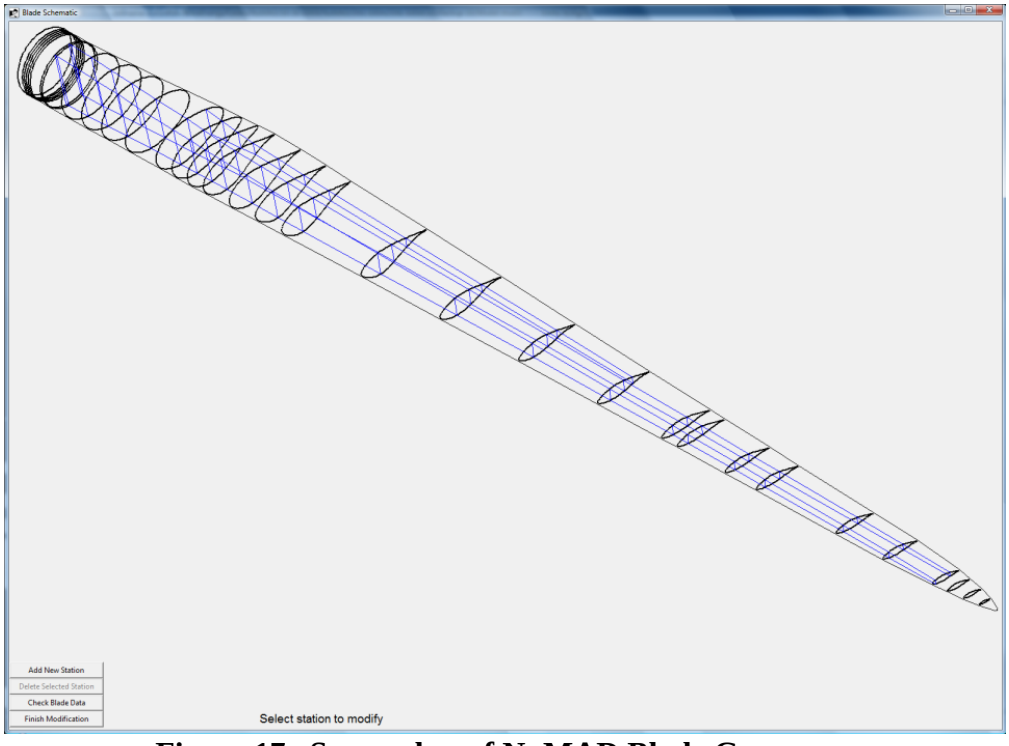

Figure 17. Screenshot of NuMAD Blade Geometry

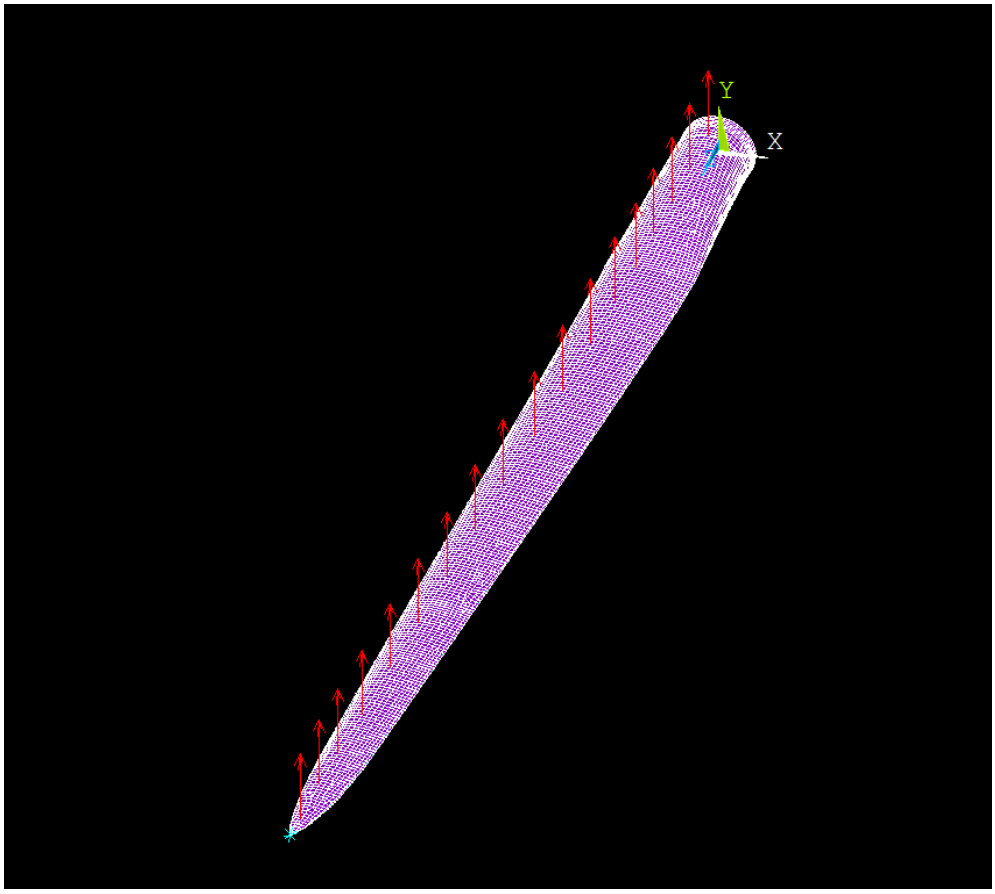

Figure 18. Loads Applied to ANSYS Structural Model for Buckling Calculation

Plots of the three lowest frequency buckling modes are shown in Figure 19. These modes have frequencies of 2.173, 2.184, and 2.229, which are all above the allowable of 2.042. Again, the frequency of the buckling mode provides a prediction of the scaling, or amplification, of the load at which buckling would occur in a region of the blade.

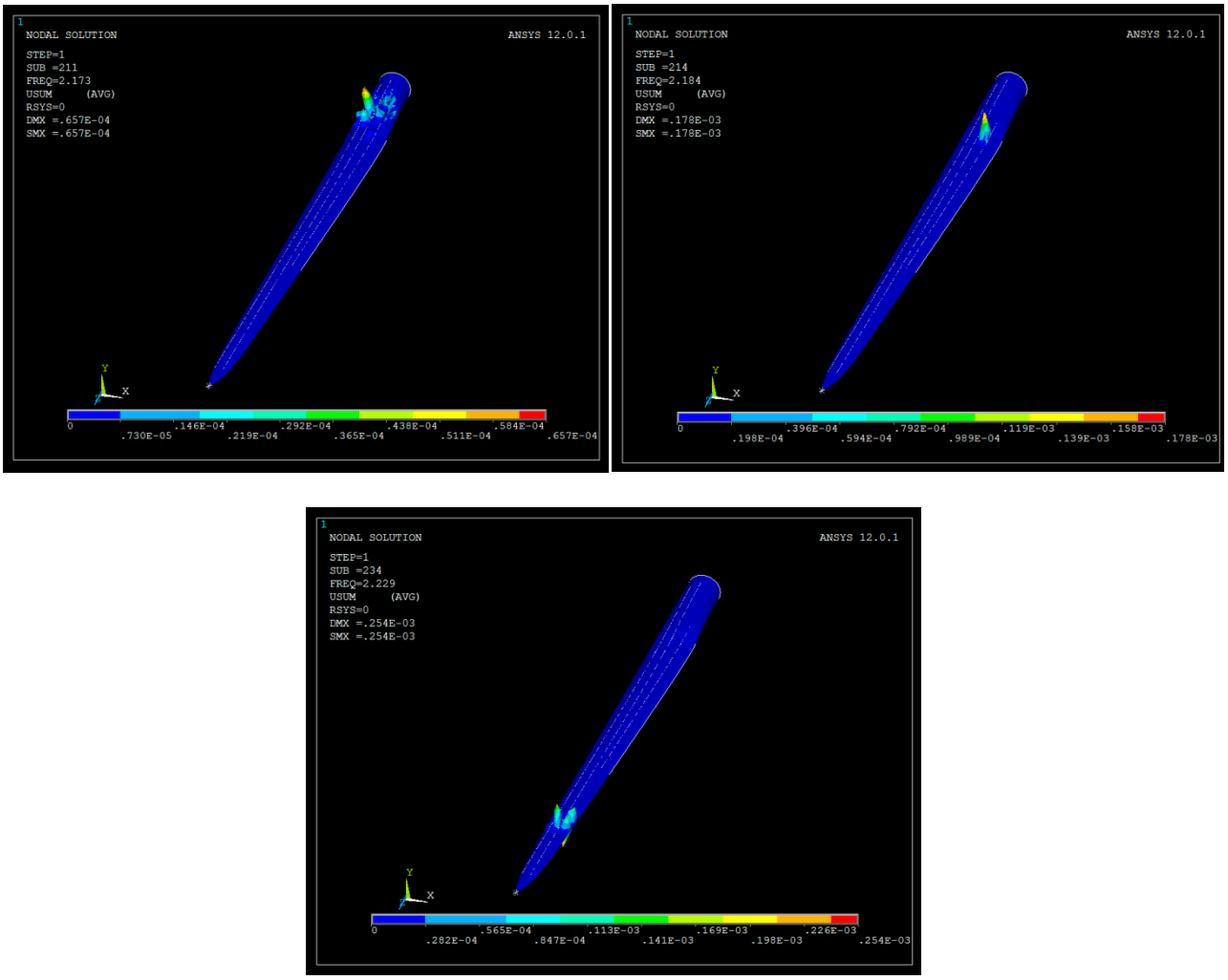

Figure 19. Plots of Buckled Shapes

A list of the principal buckling modes is provided in Table 28 with buckling frequency and a description of the location of the buckled behavior both chordwise and spanwise. This table provides a description of the load at which different areas of the blade would be susceptible to buckling under the EWM50 loading with zero degree pitch angle. The table lists the lowest frequency buckling modes that occur in the spar cap, aft panel, leading edge panel, and trailing edge panel. Efforts to improve buckling resistance in the aft panel and trailing edge reinforcement by both adding fiberglass layers as well as increasing the core foam thickness resulted in excess design margins. These design margins could be exploited to reduce blade weight in future optimization studies. Also, no buckling of the shear webs was noted in this analysis. Potential may also exist to reduce the thickness of the shear webs.

Table 28. List of Principal Buckling Modes

Frequency	Chord-wise Location	Span-wise Location
2.173	Spar cap	10 to 15 meters
2.184	Aft Panel	19.5 meters (maximum chord)
2.229	Spar cap and aft panel	72 to 80 meters (outboard)
2.327	Leading edge panel	25 to 29 meters
2.536	Trailing edge reinforcement	23 to 37 meters
2.589	Trailing edge reinforcement	19.5 meters (maximum chord)

4.5.3 Fatigue Evaluation

Fatigue properties of materials used in the 100-m baseline design were derived from test data reported in the DOE/MSU Composite Material Fatigue Database (Ref 18, pgs. 17-18). A Miner's Rule calculation was selected to predict the fatigue life of the blade. Only a single R-value of 0.1 was available for the analysis of a laminate of 66% uni-axial and 34% double bias with epoxy (denoted at E-LT-5500-EP in the DOE/MSU database). The S-N curve (failure stress versus number of cycles) for a laminate is defined by the single-cycle failure stress and the slope of the curve of the test data, if available. The fit of material fatigue test data indicates a slope parameter of b=9.13. In accordance with GL standards, a fatigue slope of b=10 was used for the fatigue analyses here.

Edge-wise strains were the driver in the fatigue life calculation. For a GL recommended slope of 10, a 1290 year life was calculated. This estimate exceeds 20 years and corresponds to a lifetime to failure at the 11.1 meter span location under edge-wise loading. Flap-wise accumulated fatigue damage was 2-3 orders of magnitude lower than edge-wise at the corresponding span-wise locations. The vast majority of laminates in the Sandia 100-meter All-glass Baseline Blade has greater than 66% uni-axial material composition, and will have higher fatigue resistance than the fatigue properties used in this analysis. Therefore, these calculations are considered conservative in this respect.

A more detailed summary of the fatigue damage calculation methodology and results can be found in Appendix A**.**

4.5.4 Flutter Analysis

Classical aeroelastic flutter of a wing (or turbine blade) is a serious condition whereby the structural and aerodynamic damping is insufficient to dampen out large vibratory motions due a coupling of flapwise (bending) and torsional (twisting) modes. It typically has not been an issue in utility-scale wind turbine designs. It has been expected, however, that the continued growth of wind turbines (greater than 10MW) would reach a point where blade flexibility and higher loads would result in aeroelastic instabilities. This would mean that aeroelastic instabilities, such as flutter, would then become one of the principal design drivers.

An estimate of the operating speed for the occurrence of a flutter condition was calculated for the 100-m baseline blade using a technique developed at Sandia for wind turbines. As expected, the flutter

mode manifested as a coupling of a flapwise and a torsional mode and occurred when the total damping (aeroelastic and structural) became negative.

> In 1984, Sandia National Laboratories (Lobitz) developed a NASTRAN-based analysis tool that incorporates aeroelastic effects and allows the user to estimate flutter speeds, divergence characteristics and levels of aerodynamic damping for various modes of vibration of Vertical Axis Wind Turbines (VAWT's) [19]. Flutter predictions were validated using field measurements of a 2-m VAWT. This technique was extended to Horizontal Axis Wind Turbines in 1998 as described in Ref. 20. Recently, Resor (21) automated the analysis procedure by developing a MatLab routine that easily sets up the NASTRAN input file and has an option to input structural properties directly from NREL's FAST and AeroDyn inputs, from a Sandia NuMAD finite element blade model or from an NREL PreComp analysis of the blade structure.

The following table lists results of flutter speed estimations for the 100-m baseline as well as several horizontal axis wind turbine blades of increasing blade length. The trend shows that the ratio of flutter speed to turbine rated operating speed drops significantly as the blade grows in length from 5 m to 9 m to 34 m and finally to 100 m. The 1.5 MW WindPACT turbine with a 34-m blade has a safety margin of 2-2.5. The 100 m (13.2 MW) blade has little or no margin on flutter speed. In the one field validation of flutter [19], the flutter speed was under predicted by only 10% for a 2 m VAWT. However, the flutter analysis technique has been primarily used as a sanity check and the accuracy is unknown due to a number of simplifications in the procedure as described in Ref. 22. A more accurate analysis tool is required when the flutter speed is indicated to be an issue.

Table 29. Estimated Flutter Speed Margins for Several Blades

Blade Length	Ratio of Estimated Flutter Speed to Operating Speed	Cited Reference for Estimation
5 m – CEB	6 : 1	Ref. 20
9-m - CX-100	5 : 1	Ref. 21
34-m - WindPACT	2-2.5: 1	Ref. 22
100-m –Sandia baseline	1.0-1.1: 1	This report

In summary, flutter appears to be an issue with the 100 m baseline design. Continuing analysis has indicated that adjustments to structural and geometrical properties can push flutter speed up in frequency away from operating speeds. For follow-on work, we must:

- Develop a refined flutter prediction tool and validate with wind tunnel and field data
- Develop flutter suppression techniques for very large wind turbine blades.

4.5.5 Summary of Analyses

The layup and geometry presented in this section for the Sandia 100-meter all-glass blade design satisfies international design standards for loads and materials. The design was not systematically optimized for weight although design trade-offs were made to reduce weight as much as possible.

To summarize:

1) The resulting design satisfies the allowable strains in both the spar cap and trailing edge with good margins.

2) Tip deflection is acceptable for the assumed overhang distance, and modest tilt and precone angles.

3) Buckling is satisfied by reinforcing the preliminary layup; primarily through thickening of the foam panels and addition of uni-axial laminates and foam in the trailing edge.

4) Fatigue life was calculated to be 1290 years based on the slope parameter recommended by GL. More certainty in the fatigue life estimate could be gained with additional data for different R-values [23].

5) Flutter speed is estimated to occur close to maximum operating speed; however, initial analysis has indicated ways to overcome this barrier by adjustments to the blade design.

5.0 Future Work

Future work would include the application of innovations for weight and load reduction to the Sandia 100-meter All-glass Baseline Blade. The use of carbon fiber, flatback airfoils, bend-twist coupling, geometric sweep, pre-bending, and active control will be considered. Additionally, the suitability of design codes for analysis of large-scale machines will be studied.

Other considerations for future work:

- documentation of a 13.2 MW reference *turbine* model using the Sandia 100-meter All-glass Baseline Blade,
- the variability of design wind conditions. Wind conditions were specified to be constant across the entire rotor (e.g. hub height wind files) which is a gross over-simplification for a very large rotor diameter. Localized effects will be important to consider for all design load cases,
- additional load cases. Loads determined from extrapolation of extreme events should be analyzed. Also, a more complex analysis of turbulent conditions including spatially-varying effects as well as a more rigorous statistical analysis of turbulence should be investigated,
- power optimization. The effect of aerodynamic twist and tip speed ratio on the maximum coefficient of performance will be considered in future studies,
- transportation. Since a 100-meter blade will be too large to be transported over the US highway system in one section, blades may need to be constructed and transported in two or more sections and assembled on site using structural joints. Therefore, the addition of joints should be considered in blade modeling.
- application of the 13.2 MW turbine model (with its 100 m blade) to the development of the model to offshore siting.
- the effect of blade length on blade buckling capacity. This is a key issue for large blades because the length of unsupported panels will likely increase. Designers will attempt to lower weight by minimizing the use of shear webs and/or optimizing panel laminate thickness and material selection to lower total blade weight.
- refined flutter prediction tool. A more accurate flutter estimation capability should be developed and validated with wind tunnel and field data. Such a tool could also support development and design of flutter suppression techniques for very large wind turbine blades.
- cost analysis trade-offs for various weight and load reduction innovations.

6.0 Discussion and Conclusions

In summary, there are a number of challenges with large blade development such as: (1) blade weight growth, (2) manufacturing and reliability, (3) material volumes/cost, (4) transportation (5) aeroelastic stability (flutter) and (6) application of offshore conditions. Many opportunities exist for research and development to enable large blades: (1) airfoil architecture, material lay-ups and material choices, (2) blade planform innovations, (3) multidisciplinary design optimization, (4) blade joints, (5) load alleviation concepts (active and passive) and (6) flutter suppression techniques. These constitute a set of the challenges and opportunities associated with large blades. This report documents a baseline 100-m blade which can be used to evaluate promising design opportunities to overcome challenging large blade design issues.

In this report, the development of a Sandia 100-m All-glass Baseline Blade model was presented. Available existing 5 MW models from DOWEC, NREL, and UpWind studies for 5MW turbine blades were up-scaled to provide a means to perform preliminary analysis for design loads. Analysis of load cases from international design standards was performed to evaluate the 100-meter blade models. The results of the present study demonstrate edge-wise strain as an important design driver for large blades.

A detailed layup and external geometry for a new 100-m blade termed the “Sandia 100-m All-glass Baseline Blade: SNL100-00” was presented. This work focuses on design and structural analysis. No aerodynamic tailoring was performed. Strength, deflection, fatigue, and stability analyses were performed. After applying partial safety factors for loads and materials, as specified by the GL standard, it was determined that this design has positive margins for the bounding load cases considered. Along with the presented analyses, areas of the blade with the smallest performance margins are identified for future development or improvement. For example, regions of the blade most susceptible to buckling, experience high operating strain, or experience large fatigue damage are noted.

7.0 References

[1] TPI Composites, "Innovative Design Approaches for Large Wind Turbine Blades Final Report," SAND2004-0074, Sandia National Laboratories, 2004.
[2] Griffin, D. A., "WindPACT Turbine Design Scaling Studies Technical Area 1 -- Composite Blades for 80- to 120-Meter Rotor," 21 March 2000 - 15 March 2001, NREL Report No. SR-500-29492, 2001.
[3] Griffin D.A. and T.D. Ashwill, "Alternative Composite Materials for Megawatt-scale Wind Turbine Blades: Design Considerations and Recommended Testing," 2003 ASME Wind Energy Symposium at the 41st AIAA Aerospace Sciences Meeting and Exhibit, AIAA-2003-0696, Reno, NV, January 2003.
[4] Hillmer, "Aerodynamic and Structural Design of Multi-MW Wind Turbine Blades beyond 5MW," Science of Making Torque from the Wind Conference, 2007.
[5] Kooijman, H.J.T., C. Lindenburg, D. Winkelaar, and E.L. van der Hooft, "DOWEC 6 MW Pre-Design: Aero-elastic modeling of the DOWEC 6 MW pre-design in PHATAS," ECN-CX--01-135, DOWEC 10046_009, Petten, the Netherlands: Energy Research Center of the Netherlands, September 2003.
[6] Lindenburg, C., "Aeroelastic Modelling of the LMH64-5 Blade," DOWEC-02-KL-083/0, DOWEC 10083_001, Petten, the Netherlands: Energy Research Center of the Netherlands, December 2002.
[7] The UpWind Project. http://www.upwind.eu .
[8] Jonkman, J., S. Butterfield, W. Musial, and G. Scott, "Definition of a 5-MW Reference Wind Turbine for Offshore System Development," NREL/TP-500-38060, Golden, CO: National Renewable Energy Laboratory, February 2009.
[9] NWTC Design Codes (FAST by Jason Jonkman). http://wind.nrel.gov/designcodes/simulators/fast/. Last modified 12-August-2005; accessed 12-August-2005.
[10] Personal communication, R.P.L. Nijssen, May 2009.
[11] Bisplinghoff, R.L and H. Ashley, "Principles of Aeroelasticity," Wiley and Sons, Inc., 1962.
[12] NWTC Design Codes (PreComp by Gunjit Bir).
http://wind.nrel.gov/designcodes/preprocessors/precomp/. Last modified 26-March-2007; accessed 26-March-2007.
[13] Personal communication, J.C. Berg, April 2010.
[14] International Electrotechnical Commission (IEC) Design Standard, IEC 61400-1 Ed.3: Wind turbines - Part 1: Design requirements.
[15] NWTC Design Codes (IECWind by Dr. David J. Laino).
http://wind.nrel.gov/designcodes/preprocessors/iecwind/. Last modified 01-September-2005; accessed 01-September-2005.
[16] Germanischer-Lloyd (GL) Design Standard, Guideline for the Certification of Wind Turbines Edition 2010.
[17] Laird, D. and T. Ashwill, "Introduction to NuMAD: A Numerical Manufacturing and Design Tool," *Proceedings of the ASME/AIAA Wind Energy Symposium*, Reno, NV, 1998, pp. 354-360.
[18] "DOE / MSU Composite Material Fatigue Database," March 31, 2010, Version 19.0, J.F. Mandell, D.D. Samborsky, Sandia Technical Report: SAND97-3002.
[19] Lobitz D.W. and T.D. Ashwill, "Aeroelastic Effects in the Structural Dynamic Analysis of Vertical Axis Wind Turbines," SAND85-0957, Sandia National Laboratories, April, 1986.
[20] Lobitz D.W. and P.S. Veers, "Aeroelastic Behavior of Twist-coupled HAWT Blades," *Proceedings of the 1998 ASME/AIAA Wind Energy Symposium*, Reno, NV, 1998; 75–83
[21] Resor, B. and J. Paquette, "Uncertainties in Prediction of Wind Turbine Blade Flutter," 49th AIAA Aerospace Sciences Meeting and Exhibit, 2011.
[22] Lobitz, D.W., "Aeroelastic Stability Predictions for a MW-sized Blade, *Wind Energy*, 2004;7:211-224.

[23] Nijssen, R.P.L., "Fatigue Life Prediction and Strength Degradation of Wind Turbine Rotor Blade Composites," Sandia Technical Report: SAND06-7810P.
[24] NWTC Design Codes (Crunch by Marshall Buhl). http://wind.nrel.gov/designcodes/postprocessors/crunch/. Last modified 01-April-2008; accessed 01-April-2008.

Appendix A. Fatigue Damage Calculation

Fatigue Damage Calculation

An analysis process is required to determine fatigue life of wind turbine blade designs. The proposed method for the calculation is to use Miner's Rule of the form:

$$Damage = \sum_i \frac{n_i}{N_F(\gamma_f \gamma_m S_i)} \leq 1.0 \qquad (1)$$

where

γ_f and γ_m are partial factors of safety for loads and materials, respectively

n_i = number of cycles at stress level S_i

N_F = number of cycles to failure

The number of cycles to failure, N_F, depends on material properties derived from fatigue testing such that, in terms of stress:

$$N_F = \left(\frac{1}{C} S\right)^{-b} \qquad (2)$$

where

C = effective single cycle strength of the material and

b = inverse of the slope of the S-N constant fatigue life curve of test data when plotted log-log; absolute value

Equation (2) can be rearranged into a logarithmic form

$$S = CN_F^{-\frac{1}{b}}$$
$$\log S = \log C - \frac{1}{b} \log N_F \qquad (2a)$$

The slope of a straight line fit through S-N test data plotted log-log is used to find b and the y-intercept of the straight line fit is related to the effective single cycle strength, C. The slope parameter b is determined from a straight line fit of fatigue test data at R=0.1 for this analysis.

Simulation and Analysis Process

Transient dynamic simulations of the operating turbine with turbulent winds from cut-in to cut-out wind speeds are performed using the FAST code. Rainflow counting of flap-wise and edge-wise bending moments are performed. These moment data are used to compute stresses based on the cross-sectional geometry and material modulus. These simulations and calculations provide values for use with Eqn (1).

Aeroelastic Simulations

First, aeroelastic simulations in turbulent inflow are performed in order to determine time waveforms of flap and edgewise bending moments at the blade root and at key locations along the blade span. The turbine in this case is pointed directly into the oncoming prevailing wind, i.e. no yaw error. The time

waveform data is processed in a rainflow counting routine, Crunch [24], and cycle amplitudes are determined. Table 1 shows the simulation settings used in the FAST fatigue analysis of the 100-m blade.

Table 1 Simulation settings.

Wind Turbine Class	Class I-B
V_{ref}	50 m/s [IEC 6.2, Table 1]
Average wind speed	0.2*Vref=10m/s [IEC 6.3.1.1]
Mean wind speeds for simulation	5, 7, 9, 11, 13, 15, 17, 19, 21, 23m/s
Turbulence model	Kaimal
Aeroelastic simulation usable record length	600 seconds
Number of turbulent aeroelastic simulations at each wind speed	12
Turbine design life	20 years

Rainflow Cycle Counting

The rainflow cycle counting process yields a list of every cycle at each amplitude. Half-cycles (incomplete cycles) are treated with a weight of 0.5. An example histogram of cycle counts versus cycle amplitude is shown in Figure 1. Notice the large concentration of high amplitude cycles for this response channel due to cyclic gravity loads in the edgewise direction.

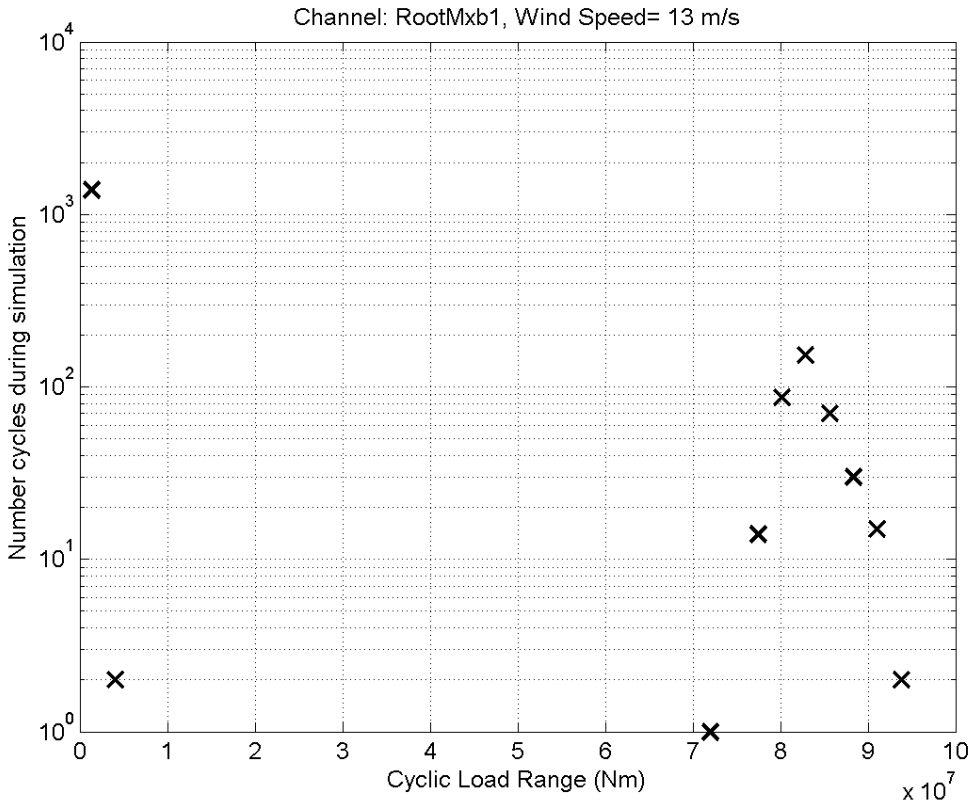

Figure 1. Cycle counts during aeroelastic simulation: Blade root edgewise bending moment.

Multiple materials at multiple locations can be evaluated in terms of fatigue. For each material/location combination, the Miner's fatigue damage is computed using Eqn (1). For simplicity, the process description written here focuses on evaluation of a single material at a single location.

Determination of Material Stress

Loads determined from the aeroelastic simulation are in terms of a moment, which relates to strain in the skin of the blade in the following manner

$$\varepsilon = \frac{Mc}{EI} \tag{3}$$

Where

M = the bending moment load experienced at the span-wise location and

c = the distance from the elastic center to the external surface of the blade skin

The section stiffness, EI, includes effects of multiple materials and the blade cross section shape. It is defined as follows

$$Flapwise, EI = \iint E(x,y)x^2 dxdy$$
$$Edgewise, EI = \iint E(x,y)y^2 dxdy \tag{4}$$

Where x and y are the flap and edgewise coordinates of the differential area elements, respectively, with respect to the section elastic center.

Also from elasticity, stress is proportional to strain

$$S = E\varepsilon \tag{5}$$

In this case, E is the Young's Modulus of a specific material which is experiencing an amount of strain computed using Eqn. (3).

The number of cycles to induce fatigue failure at the stress level given by Eqn. (5) is given as

$$N_F = \left(\frac{1}{C} S\gamma \right)^{-b} \quad (6)$$

Where

S = stress level; Eqn. (5) and

γ = combined safety factor

Determination of Cycle Accumulation Rate

Aeroelastic simulation is performed for T_{sim} at each wind speed. In this case a total of two hours is simulated at each mean wind speed listed in Table 1. The total number of cycles, n_i, at each stress amplitude, S_i, experienced in twenty years, T_{20}, at each wind speed, w, is extrapolated as follows

$$n_i = n_{i,sim} \frac{T_{20}}{T_{sim}} R_w \quad (7)$$

Where

$n_{i,sim}$ = the number of cycles counted at this load range during the aeroelastic simulation at this mean wind speed.

Note: There are two practically equivalent approaches at this point: Cycle count data can be binned such that $n_{i,sim}$ is a number typically much larger than one and the stress level S_i is representative of the center of the load range bin. Also, computing power enables rather easy summation of all cycles individually such that $n_{i,sim}$ is typically 1 (or 0.5 for a half-cycle) and the associated S_i is the actual cyclic range of the specific cycle. This work uses the later approach.

T_{20} = the amount of time in twenty years; seconds

T_{sim} = the amount of time simulated in the aeroelastic simulation from which the cycle count data are produced; seconds

R_w = the weight factor derived from the cumulative distribution function (CDF) of the Rayleigh distribution; this factor scales the cycle data at each wind speed to account for the fact that a turbine will operate at a variety of wind speeds with anticipated probability distribution at those speeds for its entire twenty year design lifetime.

The cumulative distribution function of the Rayleigh function is given by the following expression

$$\Theta = \frac{w_{mean}}{\sqrt{\frac{\pi}{2}}} \quad (8)$$

$$CDF(w) = 1 - E^{-\frac{w^2}{2\Theta^2}}$$

Where

w_{mean} = the mean hub height wind speed at the turbine installation; $0.2*V_{ref}$

The Rayleigh weights are calculated by computing the difference of the CDF evaluated at the edges of each wind speed bin. For example, R_w for the wind bin centered at the mean wind speed of 7 m/s, with a width of 2 m/s (adjacent bins centered on 5 and 9 m/s), and an average site wind speed of 8 m/s (w_{mean}=8 m/s) is found as

$$R_w = CDF(8) - CDF(6) = 0.1869$$

Fatigue Damage Calculation

Finally, the Miner's Fatigue damage at a given location on the blade for a given combination of material properties (C, b, and E) is computed as the sum of damage fractions occurring due to all cycles at all wind speeds. The fit of material fatigue test data indicates a slope parameter of b=9.13. In accordance with GL standards, a fatigue slope of b=10 was used for the fatigue analyses here.
The process is repeated for any additional materials (C, b, and E) and additional analysis locations on the blade.

Summary of Inputs

Following is a summary of important inputs used for the fatigue damage analysis.

Table 2. Table of relevant physical blade parameters at fatigue analysis locations.

	Spanwise distance from root, m	Response Channel Name	c, m	EI, GNm^2
1	0	RootMxb1	2.847	322.00
2	11.1111	Spn1MLxb1	3.833	84.57
3	15.2233	Spn2MLxb1	4.326	91.55
4	19.5017	Spn3MLxb1	4.729	105.10
5	24.2783	Spn4MLxb1	4.679	100.04
6	50	Spn5MLxb1	3.777	24.70
7	76.6667	Spn6MLxb1	2.755	7.32
8	97.7778	Spn7MLxb1	0.976	0.30
1	0	RootMyb1	2.847	322.00
2	11.1111	Spn1MLyb1	2.071	57.45
3	15.2233	Spn2MLyb1	1.805	48.94
4	19.5017	Spn3MLyb1	1.545	38.76
5	24.2783	Spn4MLyb1	1.370	29.68
6	50	Spn5MLyb1	0.718	6.26
7	76.6667	Spn6MLyb1	0.397	0.72
8	97.7778	Spn7MLyb1	0.140	0.01

Table 3. Material Properties for Fatigue.

	Material #1
Description	E-LT-5500-EP Uni-directional / DB1708 66% Uni Mar-2010, MSU Database, p.17
C, MPa	1000
b, (-)	10
E, GPa	29.38

Fatigue Damage Results

Fatigue damage results are shown in Table 4. The largest damage fraction is found in the trailing edge at the first span location beyond the blade root, Spn1MLxb1. If these values were calculated based on a twenty year lifetime, then simple extrapolation shows material at this location surviving for 20/0.0155=1,290 years.

Table 4. Miner's Fatigue Damage Results.

Miner's Fatigue Damage Values		Material #1
Edgewise Fatigue	RootMxb1	1.25E-07
	Spn1MLxb1	1.55E-02
	Spn2MLxb1	2.25E-03
	Spn3MLxb1	6.33E-04
	Spn4MLxb1	1.06E-03
	Spn5MLxb1	1.72E-08
Flapwise Fatigue	RootMyb1	1.38E-10
	Spn1MLyb1	4.88E-05
	Spn2MLyb1	3.23E-05
	Spn3MLyb1	3.13E-05
	Spn4MLyb1	3.25E-05
	Spn5MLyb1	3.50E-05

DISTRIBUTION:

Cecelia Sterling (15)
Office of Wind and Hydropower Technologies
EE-2B Forrestal Building, U.S. DOE
1000 Independence Ave. SW
Washington, DC 20585

Frank Abdi
Alpha STAR Corporation
5150 East Pacific Coast Highway Ste 650
Long Beach, California 90804

Warren Ault
LM Glasfiber ND Inc.
117 N. Jefferson Street, Suite 400
Chicago, IL 60661

Benjamin Bell
Garrad Hassan America, Inc.
45 Main Street, Suite 302
Peterborough, NH 03458

Keith Bennett
U.S. Department of Energy
Golden Field Office
1617 Cole Boulevard
Golden, CO 80401-3393

Derek Berry
NREL/NWTC
1617 Cole Boulevard MS 3811
Golden, CO 80401-3393

Gunjit Bir
Clipper Windpower Technology, Inc.
6305 Carpinteria Ave. Suite 300
Carpinteria, CA 93013

Garrett Bywaters
Northern Power Systems
182 Mad River Park
Waitsfield, VT 05673

Doug Cairns
Montana State University
Dept. of Mechanical & Industrial Eng.
College of Engineering
Bozeman, MT 59717-3800

David Calley
Southwest Windpower
1801 West Route 66
Flagstaff, AZ 86001

Jamie Chapman
Vestas Technology R&D
1111 Bagby Street, Suite 2100
Houston, Texas 77002

Joe Cohen
Princeton Economic Research, Inc.
1700 Rockville Pike, Suite 550
Rockville, MD 20852

Craig Collier, P.E.
Collier Research Corporation
760 Pilot House Dr. Suite A
Newport News, VA 23606

C. Jito Coleman
Northern Power Systems
182 Mad River Park
Waitsfield, VT 05673

Dave Corson
Altair Engineering, Inc.
634 Plank Road, Suite 205
Clifton Park, NY 12065

Scott Finn
GE Global Research
One Research Circle, Rm. K1-3C12A
Niskayuna, NY 12309

Trudy Forsyth
NREL/NWTC
1617 Cole Boulevard MS 3811
Golden, CO 80401-3393

Brian Glenn
Clipper Windpower Technology, Inc.
6305 Carpinteria Ave. Suite 300
Carpinteria, CA 93013

Dayton Griffin
Global Energy Concepts, LLC
1809 7th Ave., Suite 900
Seattle, WA 98101

Maureen Hand
NREL/NWTC
1617 Cole Boulevard MS 3911
Golden, CO 80401

Thomas Hermann
Odonata Research LLC
2813 Wild Plum Ct.
Columbia, MO 65201-3520

D. Hodges
Georgia Institute of Technology
270 Ferst Drive
Atlanta, GA 30332

Adam Holman
USDA - Agricultural Research Service
PO Drawer 10
Bushland, TX 79012-0010

D.M. Hoyt
NSE Composites
1101 N. Northlake Way, Suite 4
Seattle, WA 98103

Scott Hughes
NREL/NWTC
1617 Cole Boulevard MS 3911
Golden, CO 80401

Gino N. Iasella
Alcoa Product Design and Development
100 Technical Dr
Alcoa Center, PA 15069

Kevin Jackson
Dynamic Design Engineering, Inc.
123 C Street
Davis, CA 95616

Find Molholt Jensen
Risø National Laboratory for Sustainable Energy
Technical University of Denmark
Frederiksborgvej 399
P.O. Box 49
DK-4000 Roskilde

Simon Joncas
Ecole de Technologie Superieure
1100 Notre Dame O
Montreal, PQ H3C 1K3 Canada

Jason Jonkman
NREL/NWTC
1617 Cole Boulevard
Golden, CO 80401

Gary Kanaby
MFG
1332 Silver Hawk Way
Chula Vista, CA 91915

Dimitris Lagoudas
Texas A&M University
Department of Aerospace Engineering
710 H.R. Bright Building
3141 TAMU
College Station, TX 77843-3141

Scott Larwood
1120 N. Stockton St.
Stockton, CA 95203

Wendy Lin
GE Global Research
One Research Circle
Niskayuna, NY 12309

Steve Lockard
TPI Composites, Inc.
8501 N. Scottsdale Rd.
Scottsdale, AZ 85253

James Locke
Collier Research Corp.
760 Pilot House Dr. Ste. A
Newport News, VA 23606

John F. Mandell
Montana State University
302 Cableigh Hall
Bozeman, MT 59717

Lance Manuel
The University of Texas at Austin
Civil, Architectural and Environmental
Engineering Department-STR
1 University Station C1748
Austin, TX 78712-0273

Steve Mikel
Suzlon Wind Energy Corporation
620 3rd Avenue SE
Pipestone, MN 56164

Walt Musial
NREL/NWTC
1617 Cole Boulevard MS 3811
Golden, CO 80401

Library (5) NWTC
NREL/NWTC
1617 Cole Boulevard
Golden, CO 80401

Byron Neal
USDA - Agricultural Research Service
PO Drawer 10
Bushland, TX 79012

Chris Niezrecki
University of Massachusetts - Lowell
One University Avenue
Lowell, MA 01854-2881

Steve Nolet
TPI Composites, Inc.
373 Market Street
Warren, RI 02885-0367

Energy Research Centre of the Netherlands
T.S. Obdam
PO Box 1
1755 ZG Petten
The Netherlands

Tim Olsen
Tim Olsen Consulting
1428 S. Humboldt St.
Denver, CO 80210

Frank Peters
Associate Professor - Industrial &
Manufacturing Systems Engineering
Iowa State University
3004 Black Engineering Bldg. (mailing
address)
Ames, IA 50011-2164

Nathan Post
NREL/NWTC
1617 Cole Boulevard MS 3811
Golden, CO 80401

Ian Prowell
University of California-San Diego
9500 Gilman Drive #0085
San Diego, CA 92093-0085

Jim Richmond
MDEC
3368 Mountain Trail Ave.
Newberg Park, CA 91320

Dan Samborsky
Montana State University
302 Cableigh Hall
Bozeman, MT 59717

Scott Schreck
NREL/NWTC
1617 Cole Boulevard MS 3811
Golden, CO 80401

Brian Smith
NREL/NWTC
1617 Cole Boulevard MS 3811
Golden, CO 80401

J. Sommer
Molded Fiber Glass Companies/West
9400 Holly Road
Adelanto, CA 92301

Fred Stoll
WebCore Technologies, LLC.
8821 Washington Church Rd.
Miamisburg, OH 45069

Herbert J. Sutherland
HJS Consulting
1700 Camino Gusto NW
Albuquerque, NM 87107-2615

Andrew Swift
Texas Tech University
Wind Science & Engineering Research Center
PO Box 41023
Lubbock, TX 79409-1023

Robert W. Thresher
NREL/NWTC
1617 Cole Boulevard MS 3811
Golden, CO 80401

Steve Tsai
Stanford University
Aeronautics & Astronautics
Durand Bldg. Room 381
Stanford, CA 94305-4035

Case P. van Dam
Dept. of Mechanical & Aeronautical Eng.
University of California, Davis
One Shields Avenue
Davis, CA 95616-5294

Jeroen van Dam
WinNREL/NWTC
1617 Cole Boulevard
Golden, CO 80401

Paul Veers
NREL/NWTC
1617 Cole Boulevard MS 3811
Golden, CO 80401

Kyle Wetzel
Wetzel Engineering, Inc.
PO Box 4153
Lawrence, KS 66046-1153

Rahul R Yarala
Executive Director, Wind Technology Testing Center,
Massachusetts Clean Energy Center
55 Summer Street, 9th Floor
Boston, MA 02110

Mike Zuteck
MDZ Consulting
601 Clear Lake Road
Clear Lake Shores, TX 77565

Habib Dagher
Advanced Structures & Composite Center
University of Maine
5793 AEWC Bldg. Room 142
Orono, ME 04469-5793

Rogier Nijssen
Knowledge Centre WMC
PO Box 43
1770 AA Wieringerwerf
The Netherlands

Technical Library, 9536 (Electronic)
MS 1124 Wind Library, 6121 (20)
MS 9018 Central Technical Files, 8945-1

Internal Distribution

MS 0557 C.C. O'Gorman, 1522
MS 0346 T.J. Baca, 1523
MS 0824 J.M. Redmond, 1525
MS 0557 T.W. Simmermacher, 1523
MS 0557 D.T. Griffith, 1523 (5)
MS 1104 J.R. Zayas, 6120
MS 1124 T.D. Ashwill, 6121 (20)
MS 1124 J. Barco, 6122
MS 1124 M. Barone, 6121
MS 1124 D.E. Berg, 6121
MS 1124 J. Berg, 6122
MS 1124 G. Copeland, 6122
S.M. Gershin, 6122 (Electronic)
MS 1349 B.A. Hernandez-Sanchez, 1815
MS 1124 R.R. Hill, 6122
MS 1124 R. Jepsen, 6122
MS 1124 E. Johnson, 6122
MS 1124 W. Johnson, 6121
MS 1124 B. Karlson, 6121
MS 1124 D.L. Laird, 6122
MS 1124 M. Levy, 6121
MS 1124 B. McKenney, 6121
MS 1124 A. Ogilvie, 6121
MS 1124 J. Paquette, 6121
MS 9406 V. Peters, 6121
MS 1124 B. Resor, 6121
MS 1124 J. Roberts, 6122
MS 1124 M.A. Rumsey, 6121
MS 1124 J. White, 6121
MS 1124 J. Williams, 6121
MS 1124 D. Wilson, 6122